UNIVERSITETET I AGDER

DEVELOPMENT AND ELECTROCHEMICAL EVALUATION OF TAPE CAST SUBSTRATES FOR SOFC SINGLE CELLS

STEFFEN THOMASSEN

THESIS SUBMITTED IN PARTIAL FULFILLMENT OF THE REQUIREMENTS FOR THE DEGREE MASTER IN TECHNOLOGY IN RENEWABLE ENERGY

SUPERVISOR:
HUGH MIDDLETON

DEPARTMENT OF ENGINEERING SCIENCES

FACULTY OF ENGINEERING AND SCIENCE

GRIMSTAD, JUNE 2013

Abstract

As a means to reduce the solid oxide fuel cell material cost and make it more adapted to other fuels, titania as a candidate catalyst material has been investigated. A low-cost, high precision, self made tape casting system made it possible to fabricate thin films by the tape casting method. Substrates for SOFC single cells were manufactured through experimentation and optimization of slurry recipes for tape casting. The produced substrates were micro-structural analyzed by using an AFM, and evaluated with the use of EIS. The study shows that it is possible to fabricate standalone titania substrates. And the structural analysis and impedance spectroscopy implies that titania show desirable properties, such as amounts of porosity, good conductivity (in the order of 10^{-3} S/m) and low activation energy (0.21 eV). Still, the conductivity do not prove to be high enough, for working as the sole electronic conductor for the anode. Which is why it may be necessary to pair titania with a metallic conductor, such as copper, to reach satisfactory conductivity levels. Repeated tests are needed to further confirm the findings of this study. Further studies are also appropriate, for more extensive testing in the same track, but also to look at possible titania composites.

Preface

This master thesis fulfills the requirements for the Master in Technology degree in Renewable Energy at the Faculty of Engineering and Science in Grimstad, Norway. The practical and experimental work included in this thesis was carried out at the University of Agder.

First of all, I would like to thank my supervisor Professor Hugh Middleton for his positivism, support and guidance despite my minor knowledge in chemistry to start with. The project came to include much more chemistry than I initially expected, which has been a huge challenge for me. However, Hugh has taught me a lot during the project period, and I am very grateful for his nonjudgmental approach towards my lack of experience in this field. Thanks for the conversations, both related and non-related.

Secondly, I would like to thank Roy Werner Folgero for his technical insight and CNC-milling during the design process of my tape casting device. A big thanks to Stein Bergsmark for his valuable feedback on my report during the project. Huge thanks goes to my dear friend Faye Saint Laurent for taking the time to proofread my English. And thanks to my fellow students for the company down the road.

Lastly, warm thanks goes to my friends and my family for their support, distractions and encouragement during my studies. It has been like a gentle pushing and supporting hand behind me, especially at times when my days felt heavy and my goals seemed to be far away. Thank you so much.

Grimstad, June 2013

Steffen Thomassen

Contents

List of Figures

List of Tables

Abbreviations

8YSZ	8 % yttria stabilized zirconia.
AFM	atomic force microscope.
APU	auxiliary.
CAD	computer-aided design.
CNC	computer numerical control.
ECM	equivalent circuit model.
EIS	electrochemical impedance spectroscopy.
FC	fuel cell.
FT	Fischer-Tropsch reaction.
GDC	gadolinium doped ceria.
HOR	hydrogen oxidation reaction.
IS	impedance spectra.
LSC	lanthanum strontium cobaltite.
LSCF	lanthanum strontium cobalt ferrite.
LSF	lanthanum strontium ferrite.
LSM	lanthanum strontium manganate.
MEA	membrane electrode assembly.
MIEC	mixed ionic electronic.
MPP	maximum power point.
NC	non-contact.
NiO-YSZ	nickel oxide - yttria stabilized zirconia.
OCV	open circuit voltage.
PVA	polyvinyl alcohol.
RT	room temperature.
SDC	samaria doped ceria.
SEM	scanning electron microscope.
SMSI	strong metal support interaction.
SOFC	solid oxide fuel cell.
STC	standard-state conditions.

TEC	thermal expansion coefficient.
TPB	three phase boundary.
WGS	water gas shift reaction.
XRD	x-ray diffractometer.
YSZ	yttria stabilized zirconia.

Chapter 1

Introduction

In this chapter an introduction to SOFCs is given and a short explanation of how it works. It gives a quick insight to some of the challenges research and development faces, and which contributions that could lead to commercialization of the technology. As a goal to contribute in the research, the project is set to examine a possible anode material additive. Section 1.1 includes the background and motivation of the thesis. Section 1.2 presents the working principle of the SOFC and a description of its constituents. Section 1.3 describes some of the equipment used in this project. Section 1.4 introduces the thesis definition where the main objectives of the project are specified. In section 1.5 limitations for the project are listed. Section 1.6 discusses the contribution and importance of the work performed in this project. Lastly section 1.8 outlines the rest of the remaining chapters of the report.

1.1 Background and Motivation

As time goes by, the attention towards the climate and our earth's well-being grows stronger. It becomes obvious that measures are needed to reduce the footprints left behind, as new generations reach for the baton. As a result, research and development are conducted on numerous fields as we speak, where they contribute to an ever growing, greener mentality.

Solid oxide fuel cells (SOFC) are one of the most promising and important technologies in the field of developing fuel cells (FC). Offering clean and environmental friendly conversion of energy, without combustion and with little or no emission of pollutants. And with its high efficiency, high temperature exhaust heat and fuel adaptability, the SOFC is suitable for a number of applications. One of its strong advantages is the opportunity to utilize both its electrical and thermal generated energy, known as co-generation. First and foremost the SOFC is suitable for stationary power

generation systems, secondly it is apt as auxiliary power units (APU) and hopefully with time, also as a transportation APU.

Because of the high temperature the SOFC is tolerant for different fuels. Current and most common models works very well with hydrogen as they are, and several systems being developed can work directly on light hydrocarbons, such as LNG (methane), propane and butane. For these systems, steam reforming (explained later) happens internally in the cell, which is a required process for using hydrocarbons as fuel. SOFCs can also be fueled with heavier hydrocarbons, such as gasoline, diesel, and biofuels, but it would require these to be externally reformed before being applied.

The development of a single cell depends somewhat on the choice of materials and their characteristics. The main components, the anode, electrolyte and cathode, must have certain matching properties. One of the three components normally act as the main supporting substrate and give mechanical strength to the single cell. This supporting layer is often a governing factor for the final single cell design, where the layer's electrochemical and mechanical properties are influential factors.

Mapping the characteristics of SOFCs single cells and substrates can be done in several ways. One method that has gained huge popularity in the last decade is electrochemical impedance spectroscopy (EIS), also known as AC impedance spectroscopy. With this tool one is able to measure the impedance of the FC, and because the impedance is influenced by many of the electrochemical processes in the FC, one can relate and learn about these processes by analyzing the measured impedance data.

For commercializing the SOFC without reducing its efficiency and performance, there are many tasks and challenges to be tackled along the road. Where the aims are to improve performance, extend the range of its applications, reduce production costs and prolong its operational lifetime. Production methods and the choice of materials are therefore playing a significant economic and qualitative role in the search for improvements.

1.2 The Solid Oxide Fuel Cell

The main components of the fuel cell, the anode and cathode with the electrolyte sandwiched between is the membrane electrode assembly (MEA). An illustration is given in Figure 1.1. The MEA is placed between two current collecting end plates, which also incorporates fuel and air flow fields. For pairing multiple single cells together into a FC stack, interconnections (bi-polar plates) are used between the cells as a part of the external electric circuit.

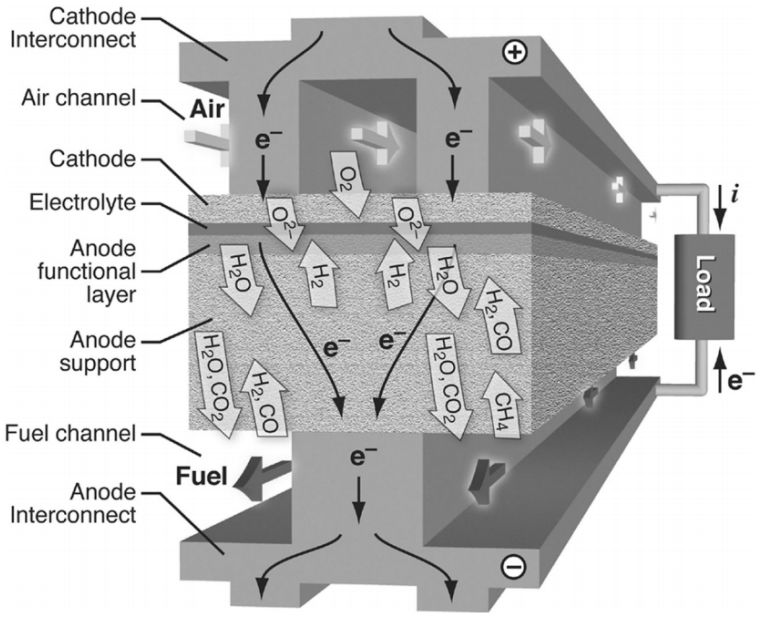

Figure 1.1: Section of a planar membrane-electrode assembly (MEA), illustrating essential fluid, chemical, and electrochemical processes [12].

1.2.1 Working principle

The electrochemical reactions in the SOFC directly converts the chemical energy of a fuel into electrical energy. The fuel is oxidized at the anode side and the electrons are transported over to the cathode side through an external circuit containing the load. On the cathode side, the reactant together with the incoming electrons are reduced to ions (O^{-2}) which are transported through the gas tight ionic conducting electrolyte (YSZ). At the anode side the ions combines with the fuel and produces the combustion product. The electrochemical half reactions which occur in a H_2-O_2 solid oxide fuel cell are as follows and illustrated in Figure 1.2:

$$Anode: \quad H_2 + O^{2-} \rightarrow H_2O + 2e^- \tag{1.1}$$

$$Cathode: \quad \frac{1}{2}O_2 + 2e^- \rightarrow O^{2-} \tag{1.2}$$

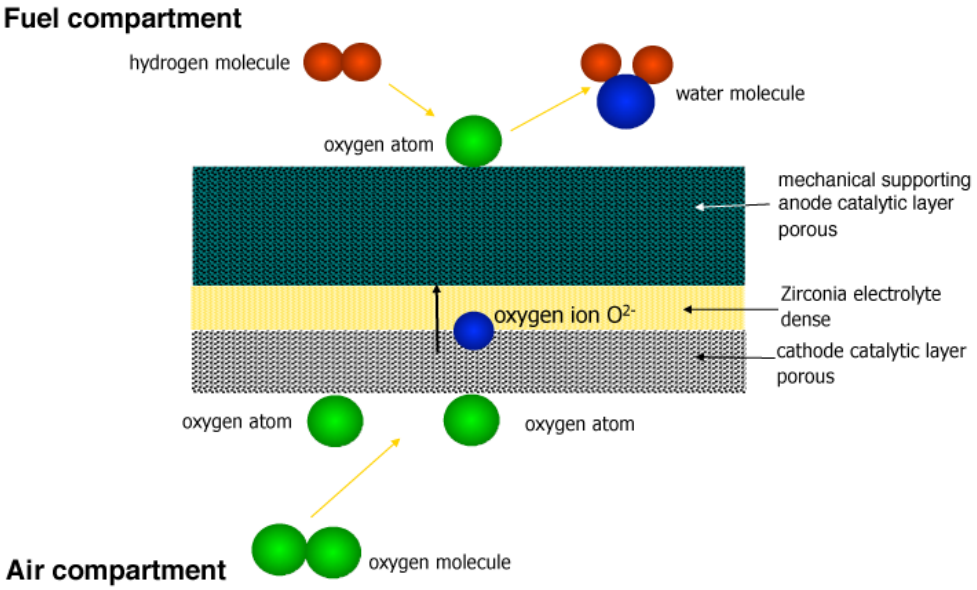

Figure 1.2: Chemical reactions in a H_2 - O_2 fueled SOFC [27]

1.2.2 Solid Electrolyte

Yttria-stabilized zirconia (YSZ) is a ceramic material that is the most commonly used SOFC electrolyte, both in research and development. It is a gas tight ionic conducting solid oxide, which separates the fuel and reactant gases. Since the solid electrolyte only conducts ions at high temperatures, the FC usually operates between 750 - 1000 °C. To develop the SOFC towards more commercial markets, it is desirable to improve the fuel adaptability, with focus on performance and FC lifespan. Since the ionic conductivity is a function of temperature, the electrolyte thickness is reduced, also as a measure for avoiding increasing ohmic losses. In earlier versions, the electrolyte was working as the mechanical supporting layer for the cell, but in the quest to reduce performance losses the thickness has been decreased, and the role as a supporting layer has been shifted to the electrodes.

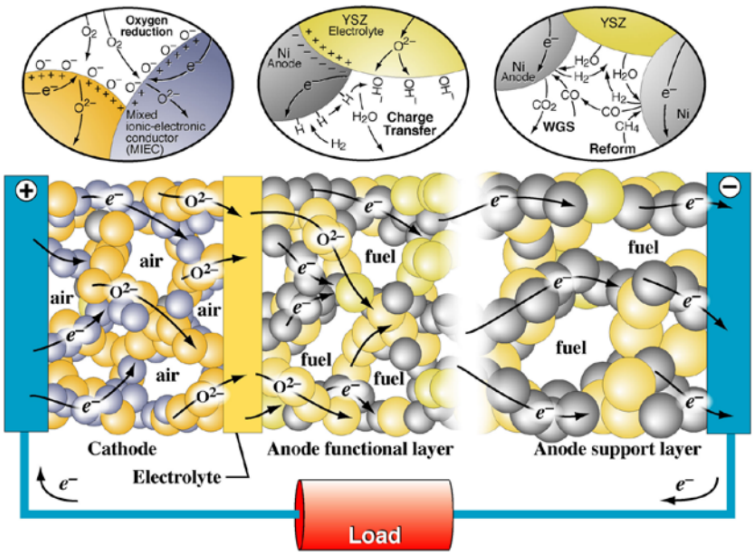

Figure 1.3: Microscopic representation of a MEA in the vicinity of the dense electrolyte. For this case there is a double-layered anode. [12].

1.2.3 Anode

The anode must be a very good catalyst for oxidation of the incoming fuel. For good transportability of both the fuel to and the exhaust product away from the electrolyte, the anode layer need an adequate amount of porosity. Other requirements adds to match the electrolytes thermal expansion coefficient, which leads to good adhesion between the two. The state-of-the-art anode material is a two phase nickel and yttria-stabilized zirconia cermet, where nickel offers excellent catalytic properties and good operational stability. In higher quantities, over 30 %, nickel gives mechanical strength and increasing electron conductivity to the anode layer. Most often the anode electrode is chosen as the mechanical supportive layer for SOFC, when the electrolyte is not.

1.2.4 Cathode

The cathode needs to meet the requirements of high catalytic activity for oxygen, high electronic conductivity and low reactivity with the electrolyte. As development has lead to find cheaper catalyst materials, perovskites has become a commonly used class of ceramics instead of expensive noble metals. The formula which distinguish the perovskite class is of the form $X^{2+}Y^{4+}O_3$. Due to its similarity in crystalline structure, the class has its name from a specific mineral with the same structure, known as perovskite ($Ca^{2+}Ti^{4+}O_3$). As an oxide, the perovskites hold both good ionic and electronic conductivity. Lanthanum strontium manganate (LSM), lanthanum strontium ferrite (LSF), lanthanum strontium cobaltite (LSC) and lanthanum strontium cobalt ferrite (LSCF) are some of the typical cathode materials being used today.

1.3 Equipment Description

This section gives a short description of some of the equipment that were used during the project which will not be described in any further detail.

3D printer - as the name implies, a printer that prints three-dimensional models which are first created on a computer in a typical 3D modeling CAD application, such as Autocad, Inventor, SolidWorks. The printer builds the model layer by layer in the XY-plane, and some printers also print a soluble support structure that allows it to print structures in midair. The typical printing material is nylon and comes in a variety of colors. Low-end printers use only one color while working, while high-ends can do multi-color printing.

Ball mill - Is a type of grinder that is used to grind crushed materials into very finer powder. This can be done either in dry or wet conditions. The construction is made up of a cylindrical container with numerous dense, heavy steel or ceramic balls. The container turns around with a certain speed, so that the balls as a result of the centrifugal force, is raised up to a point where they fall down with a crushing force. The rotating force usually come from gears connected to the container. Or for smaller mills, the container rest on two rollers where one of them are mechanical rotated, which is the case in this project.

Atomic force microscope (AFM) - Is a very high-resolution type of scanning probe microscope, which can scan a sample at the resolution on the order of a fractions of a nanometer. The microscope uses a micro needle, so called cantilever, to gather information from the sample, by feeling its surface. This is also done in a raster pattern to produce the image of the scanned area. The microscope has several scanning modes, but the main are Contact-, Non-Contact- (NC) and Intermittent NC mode. In contact mode, the cantilever scans the sample by being in contact with the sample. In Non-Contact mode, the cantilever is oscillated above the sample, gathering information by for example being influenced by van der Waals forces. In Intermittent NC mode, the cantilever additionally taps on the sample, allowing density information to be gathered. The changes influenced on the cantilever is measured using a laser spot deflecting the top surface of the needle [4].

1.4 Thesis Definition

Examine the possibility that titania (TiO_2) may function as a catalyst in the anode of a solid oxide fuel cell.

Main goals:

1. Design and build a high precision multilayer tape casting system.
2. Investigate and optimize formulations for making slurries for the tape casting setup (such as YSZ, NiO-YSZ and TiO_2).
3. Carry out micro-structural analysis of prepared substrates using AFM. Furthermore perform I-V characterization (complete single cell), AC impedance spectroscopy, thermal and redox observations.
4. Optimization of the substrates by iterating the fabrication process with the help of the performance and robustness testing.
5. **If time allows:** Develop a robust structure that can be incorporated in a SOFC single cell.[A]

Evaluation and test programme:

1. Micro-structural analysis with AFM on unsintered substrates.
2. Measure substrate shrinkage after sintering.
3. Micro-structural analysis with AFM on sintered substrates.
4. Characterize current and voltage behavior (complete single cell).[A]
5. Collect impedance spectra from substrates with AC impedance spectroscopy.
6. Observe if substrates handle redox and thermal cycling.

1.5 Project Limitations

- The SOFC cathode is not within scope of this project and will not be widely covered.
- The project is limited to substrates and single cell FC testing.
- There will not be enough time for extensive in-depth electrochemical testing.

1.6 Contributions to the scientific society

The project has brought forward and demonstrated a low-cost, high precision tape casting tool. Furthermore, this work has shown that it is possible to create standalone titania substrates for evaluation.

1.7 Report Outline

The remaining part of the thesis is organized as follows. Chapter 2 introduces the theoretical background for SOFC and common materials, and presents methods for production and electrochemical evaluation of these. Chapter 3 explains how designing, production and electrochemical evaluation was performed. Chapter 4 presents the experimental results from the study, characterizations of the FC samples, impedance spectra and micro-structural analysis. Chapter 5 discusses and evaluates the results. Chapter 6 concludes the thesis and comments the main goals.

Chapter 2

Theoretical Background

This chapter introduces slurry production theory and the methods used for slurry deposition. It also explains the SOFC and its theory, along with a presentation of titania and the most commonly used SOFC materials. Lastly the chapter concludes a description of the theory behind electrochemical evaluation and the respective equipment applied to this.

2.1 Tape Casting

Tape casting is a widely used low cost production method, which uses a doctor blading device to apply a thin film of a well-mixed slurry of some sort unto a cast carrier e.g., a glass plate. There are mainly two ways to do this, one is to have the doctor blading device move along the cast carrier, the other is where the cast carrier moves under a fixed doctor blading device. The first method is described as a discontinuous process, and the second a continuous one. The continuous process is normally used for big scale productions, where the moving carrier often is a flexible belt of stainless steel or plastic films driven by a motor. The minor production this experiment pose, makes the discontinuous method most suitable by using a small film-applicator. The anode substrate and the electrolyte will be tape casted, while the cathode is fabricated by screen printing.

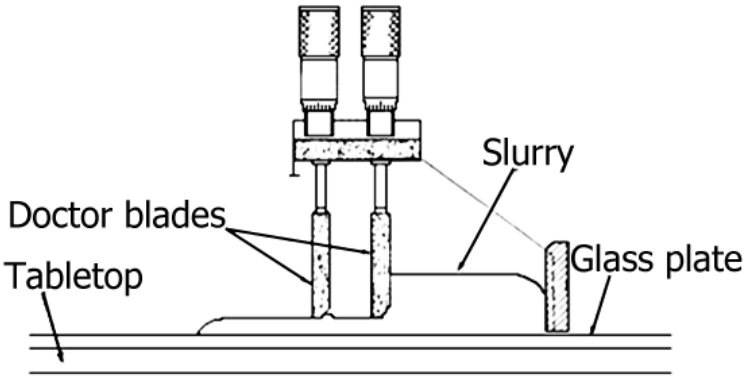

Figure 2.1: Illustration of tape casting technique [29].

Screen printing is often combined with tape casting and is done much in the same way as amateurs screen print t-shirts. It is also a well used low cost manufacturing process, that can produce SOFC layers in the desired thickness down till about 10 - 20 µm. Where the result depends on the quality of the equipment, printer settings, screen options, slurry preparation and ink/slurry rheology. Dollen and Barnett [5] reported good results from their screen printing study, where the OCV of their SOFC was close to that of the theoretical SOFC voltage of 1.1 V.

For an anode supported MEA composition, the anode is the thickest part of the fuel cell and acts as the mechanical support for the entire MEA. Production of the single cell begins with a very thin electrolyte layer, then afterwards a thick, porous anode layer is spread across it. Depending on the production process, the order in which it happens can vary. Lastly, usually after sintering, a thin cathode is deposited on to the other side of the electrolyte. Sometimes the single cell will be cast as a tri-layer, as a complete MEA before it is sintered. Other times the anode and electrolyte will be co-casted together, sintered and the cathode added later. An example of the SOFC component composition is shown in Figure 2.2.

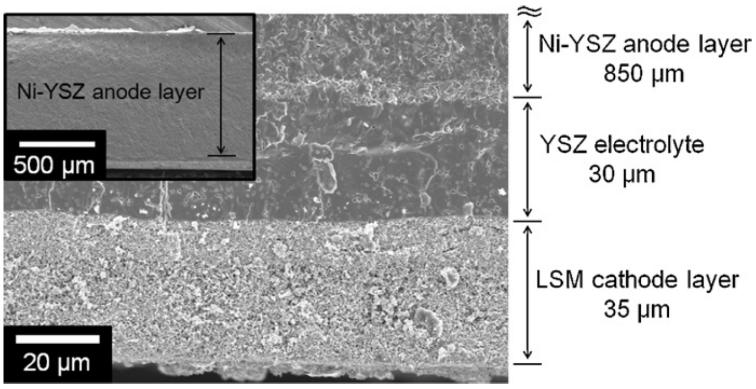

Figure 2.2: Cross-sectional SEM image of an anode-supported button cell [11].

Cracking and delamination can sometimes be a problem with anode supported MEAs, and it has

also been shown to increase the fuel mass transport resistance. On the other hand, a thicker porous anode layer has been revealed beneficial when hydrocarbons are directly fueled to the FC, since it increases the fuel residence time in the anode, thus increasing the conversion capacity [30]. In other words, a thicker anode layer can improve the performance of a hydrocarbon fueled FC. As a result of this and despite some of the disadvantages, the anode supported MEA is favored among other alternatives, because it has been the design that has proven best performance.

2.1.1 Slurry Formulation

Table 2.1: Formulation template

Ingredient	**Description**
Powder	YSZ
Solvent	Distilled water
Binder	PVA (polyvinyl alcohol)
Plasticizer	Glyserol
Dispersant	Tween 80
Defoamer	Propanol

A good **powder** is finely milled. That is, a powder with uniform particle size, which is one factor that increases the reliability of the tape casting process. As a result, it will dissolve well in the solvent and spread evenly throughout the slurry with the help of other additives. Smaller particle size, yield higher tape density. Nevertheless, smaller particle size leads to a higher degree of tape shrinkage due to increased specific surface area. This is not advantageous, since it requires higher concentrations of additives [7]. And higher concentrations of additives can lead to increased deformity during drying and sintering. The properties of the end result has to be taken into consideration, because some layer properties depends on the density. For an SOFC electrolyte it is desirable to have a dense layer, since no gas or fluid is suppose to transfer through it. While for the anode layer, it is desirable to have a porous layer, so that gas can seep through it. For that case, coarser particles are needed to create porosity and a lesser dense layer.

The **solvent** dissolves the organic materials and is usually the main contributor in liquifying the slurry. Depending on what kind of solvent that is being used, it can highly influence the rheology. The main purpose of the solvent is to evenly distribute the materials throughout the slurry and being a transporter until it vaporizes and leave behind a dense tape [7].

The **binder** is the glue in the slurry, making the casted tape stick together. It also works as the hardener. Binders affect the rheology of the slurry, increasing the viscosity and changing its characteristics. Too little will make the cast tape form cracks when it dries, while too much on

the other hand will fill it with voids. Something else to mention is, with an increasing amount of binder the strength of the tape increases too, while density decreases as seen in Figure 2.3 [7].

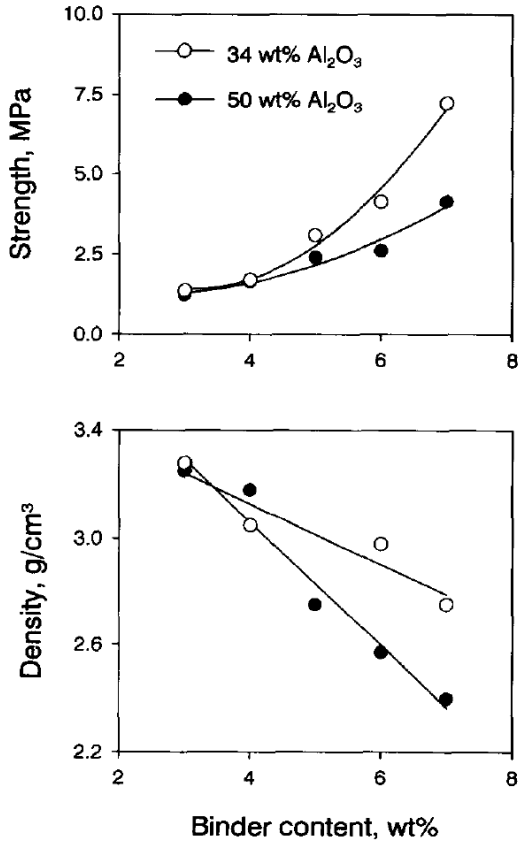

Figure 2.3: Strength (top) and density (bottom) of alumina green tapes with different powder charges as a function of HEC wt.%.[7]

Adding **plasticizer** to the slurry softens the binder and makes the cast tape flexible, manageable and shapeable in the dry or semi-dry state. Without it or too little, will make it difficult to handle or edit the tape in any way. E.g. when separating the thin tape from the cast carrier. Strain it a little too much and it will break or tear. On the other hand, too much plasticizer can reduce the tapes strength [7] and over-soften the binder.

A **dispersant** agent also called a deflocculant, coats the ceramic particles which resists them from sticking together. Flocculation is small particles bonding to each other in the form of a flake. If they become big enough in size, the gravitational forces will eventually influence them and cause sedimentation. In the flat microstructure of a SOFC single cell, such a flake would be characterized as an agglomeration, and is a unwanted electrochemical interfering defect. It is desirable to have the particles well spread and in stable suspension, making up a homogeneous slurry [7].

The **defoamer** is a chemical additive that counteracts the formation of foaming in liquids under production or processesing. If there is a lot of foam or bubbles in the slurry when it is casted, the

result will likely contain imperfections and weaknesses. The goal is to produce a uniform smooth film without bubbles and agglomerations.

2.1.2 Titania

The normal and most stable oxidation state of titanium is +4 valence electrons. At room temperature titania (TiO_2) shows high electrical resistance and results in very low electron transfer rate, thus not a suitable conductor, but is popularly used as insulator for capacitors. In a reducing hydrogen or carbon atmosphere, it will start to loose oxygen ions upon heating.

$$TiO_2 + H_2 = TiO + H_2O \tag{2.1}$$

$$TiO_2 + CH_4 = TiO + H_2 + CO \tag{2.2}$$

By reduction reaction, oxygen vacancies are created and can be described by the nonstoichiometric form:

$$TiO_{2-x} \tag{2.3}$$

which gives Ti^{3+} or even Ti^{2+}. In reduced state titania is "activated" as an electron donor and turns into a n-type semiconductor. With the temperature rising past 300 and towards 1000 °C, the number of contributing electrons will increase as the present oxygen ions decreases. Subsequently titania will act as an n-type semiconductor with increasing conductivity. Reducing titania(r) even more, to a monoxide,

$$TiO_{2-1} = TiO \tag{2.4}$$

something interesting is formed in the crystalline structure. Something called shear structures or -planes, known to titanium oxides with the composition of:

$$Ti_nO_{2n-1} = Ti_1O_{2-1} = TiO \tag{2.5}$$

This form of titanium oxides is known as Magnéli phases, and has received a lot of attention due to their special properties of thermal, electrical and metal-nonmetal transition. When stoichiometric titania is activated and becomes conductive, it is attributed to n-type electronic conduction. On the other hand, when titania Magnéli phases begins to conduct, it is with respect to electrical conductivity. As Regonini et al. explains it, "Pure Ti_nO_{2n-1} is a (semi)metallic-type conductor, hence there is no thermal activation and an increase in resistivity with increasing temperature would be expected." [32].

By introducing titania to the cermet anode, it could hopefully reduce the amount of nickel in the common existing NiO-YSZ substrate. It may be possible to have a look at how TiO_2 works together with NiO-YSZ, how it influence and change the electrochemical and mechanical properties of the substrate, but also how it can affect a complete single cell. The thermal expansion coefficient of sintered titania is 9 x $10^{-6}K^{-1}$ (RT - 1000 °C) [24].

2.1.3 Electrolyte Components

Zirconium oxide (ZrO_2), also called zirconia, is difficult to keep stable at room temperature after it has been sintered. Due to temperature changes it will transition between certain crystalline structural phases, which leads to large volume changes. Thermal expansion is a huge challenge in fuel cell design. Parts of different materials and composites are fitted together, where they need to operate within equal displacement margins. If this is not satisfied, the final product will indeed have a short operational lifetime after a number of thermal cycles due to difference in thermal expansion.

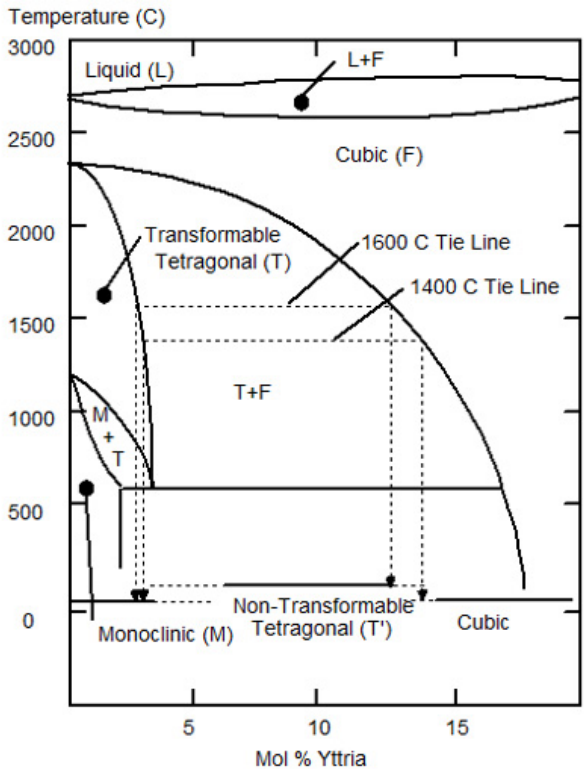

Figure 2.4: Phase diagram for the Zirconia Yttria System [8].

Doping zirconia with yttrium oxide (Y_2O_3/yttria), does two things. It stabilizes and lowers the zirconia phase transitioning, allowing it to sinter with cubic structure in the tetragonal domain. This is possible due to the lowering of phase transition boundaries, where the tetragonal phase is lowered to monoclinic domain, and the cubic to the tetragonal. By being stabilized, zirconia will keep its sintered cubic structure during temperature changes. This helps to reduce the thermal expansion, thus countering several issues appearing after numerous thermal cycles. Such as thermal cracking and the delamination between layers, to mention a few. What yttria does in addition, is creating oxygen vacancies in the zirconia lattice. As shown in Figure 2.5, it happens as a result of Y^{+3} ions replacing a number of Zr^{+4} ions. Wherefore three O^{-2} ions replaces four, one vacancy arises, hence YSZ obtains O^{-2} ion conductibility.

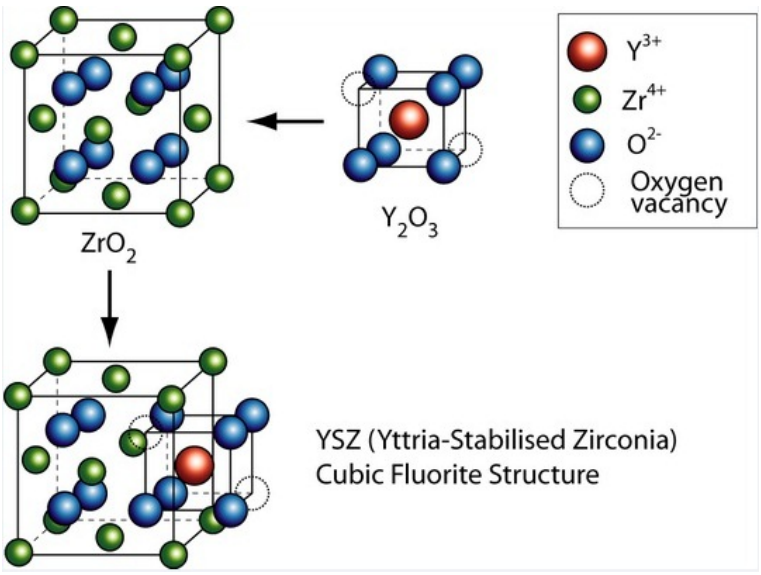

Figure 2.5: Illustration of yttria-stabilized-zirconia structure [29].

Through research it is found that different concentrations of yttria yield different properties in zirconia, where the main features are mechanical strength and ionic conductivity. Depending on the design of the fuel cell, a choice has to be made on which of the properties are most favorable. Since the SOFC for this project is anode supported, it is desirable that the electrolyte has as high ionic conductivity as possible. The illustration below, Figure 2.6, is a simple attempt to describe the correlation between concentration of yttria and the features of the doped zirconia. 8% concentration of yttria has been found to yield the maximum conductivity in YSZ. Increasing the concentration past this value will tip the scale and result in lower conductivity.

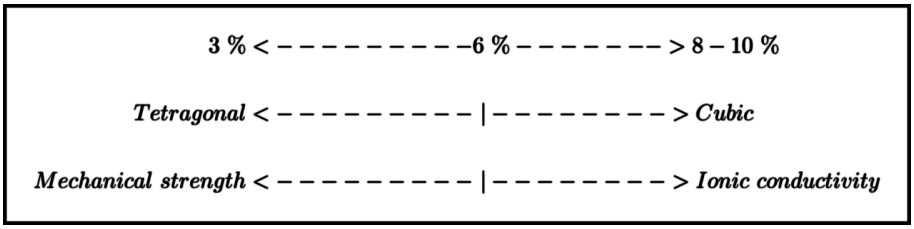

Figure 2.6: Illustration of YSZ features depending on yttria concentration.

The averaged thermal expansion coefficient between 298 and 1273 K were reported by Yasuda and Hishinuma to be (10.3 - 10.5) x $10^{-6}K^{-1}$ for 8 mol% YSZ [6].

2.1.4 Green Tape Components

As a result of nickels good electronic conductivity, stable and high catalytic activity, nickel oxide-yttria stabilized zirconia (NiO-YSZ) has become the state of the art anode substrate. During op-

eration, the oxide composite is reduced to Ni-YSZ when exposed to the fuel. Reduced to nickel metal, the cermet obtain porous structure, electronic conductivity and catalytic activity. YSZ on the other hand provides a structural skeleton, offer thermal expansion similar to the electrolyte and behaves as a nickel agglomeration restrainer.

By combining YSZ with nickel, ionic conductivity is added to the anode and extends the triple phase boundary length in the interface with the YSZ electrolyte. The TPBs, are where the gas phase, ionic- and electronic conductors are in contact. Higher number of TPBs, yield higher electrochemical performance and lowers the FC activation energy. As shown in Figure 2.7, to attain good electronic conductivity, the percolation threshold for nickel lies around 30 %. Any lower concentration will result in a higher ionic instead of electronic conductivity [30, Ch.9].

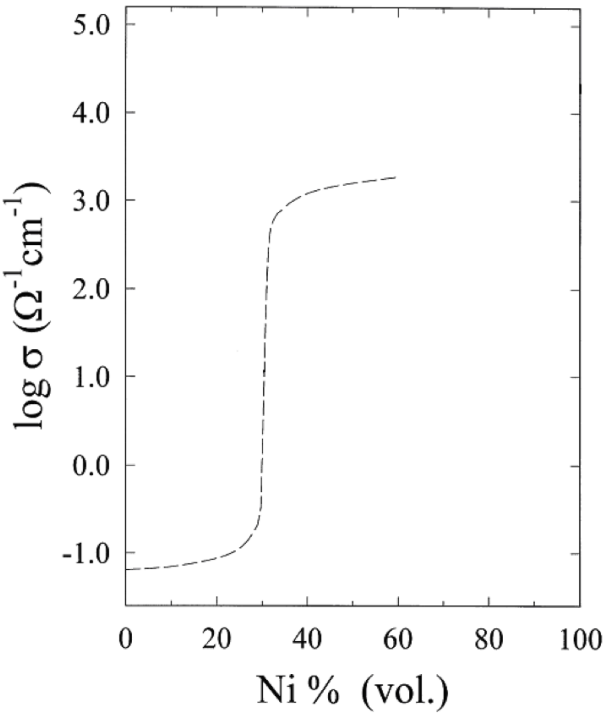

Figure 2.7: Conductivity as a function of vol% nickel [27].

Despite nickel's good properties, it has several disadvantages too. It is expensive and also toxic. The cermet anode has issues with nickel sintering, which is enhanced by long operation time, impurities in the fuel and frequent redox and thermal cycles. The result is a reduction in the amount of triple phase boundaries and electronic conductivity. Another disadvantage is when the SOFC is fueled with hydrocarbons, such as methane (CH4), because nickel works as a catalyst to formation of carbon fibre. A process known as the Boudoir reaction (2.8). Carbon depositions induce rapid cell degradation, where it decreases the anodes conductivity and in the end deactivates the anode catalyst, leading to cell failure.

Often an external reformer is used to steam reform the hydrocarbons before it is fed to the fuel

cell, a reaction known as the Fischer-Tropsch (FT) synthesis (2.6). Feeding the FT product directly to the FC will over time result in carbon depositions. A typical way to counteract the Boudoir reaction is to humidify the FT reformat with steam, before it is fed to the FC. Carbon monoxide reacts with the water vapour, and more H_2 is formed in the reaction, which is known as the water gas shift reaction WGS (2.7). This way the carbon is bound as CO_2 instead of CO, there is an increase in hydrogen energy and the chance for single carbon products is reduced. The frequency these reactions occurs by, strongly depends on the characteristics of the catalyst and the operating temperature [17].

$$CH_4 + H_2O \rightarrow 3H_2 + CO \tag{2.6}$$

$$H_2O + CO \rightarrow H_2 + CO_2 \tag{2.7}$$

$$2CO \rightarrow CO_2 + C \tag{2.8}$$

However, adding steam to the processes has its own disadvantages, owing to the fact that it can accelerate nickel agglomeration, and in some amount dilute the fuel, causing a lower efficiency [30]. For that reason it is desirable to reduce the amount of steam in the fuel, and in that way gain a higher efficiency and more durable FC operation.

One suggestion for how this could be solved, is by replacing a quantity of the nickel with other oxides in the cermet. Replacing a portion of nickel with titania (r) could reduce the Bell-boudoir reaction, and subsequently allow a lower steam/fuel ratio. Several surveys claims in various degree that titania can suppress nickel sintering in the cermet [15, 16, 34], as the presence of TiO_2 tend to extend the performance of the FC [35]. It is reported that TiO_2 has a tendency to form strong interfacial bonding with nickel, where the result is termed strong metal support interaction SMSI. Tiwari and Basu's [37] study found the following: "As X-Ray Diffraction analysis revealed that Ni, TiO2 and YSZ retain in their individual phases, it is expected that the synergistic effect of TiO2-Ni through SMSI may have prevented Ni coarsening and loss in interconnectivity and cell performance during several redox cycles". The NiO-YSZ cermet TEC highly depends on NiO concentration, with its (14.1 - 14.2) x 10^{-6} °C^{-1} TEC compared to YSZs TEC of (10.3 - 10.5) x 10^{-6} °C^{-1} [28].

2.1.5 Cathode Components

The cathode is not within the scope of this project and will not receive extensive attention, there is however some areas worth mentioning.

Lanthanum strontium manganate is a much used cathode material, much for the reason of its good compatibility with YSZ electrolytes due to its stable chemical interface reactivity and matching TEC). Apart from that, it has excellent electronic conductivity and high catalytic activity at high temperatures. At lower temperatures LSM shows poor polarization properties (activation-, ohmic losses) ($\leq$800 °C), and may not be the best choice for an intermediate temperature SOFC. However, the medium-temperature performance for LSM can be improved by adding a second ionic phase to the cathode, such as YSZ or gadolinium doped ceria (GDC). A LSM-YSZ cathode composite has proved promising results, with increase in electrochemical activity as a result of extended TPBs in the interface with the YSZ electrolyte [21].

Another alternative is LSCF, a ceramic material from the ferrite perovskite group, which has through study demonstrated good results at low temperatures [13]. It seems to be a good candidate for intermediate temperature applications, and could be the better choice over LSM because of its higher catalytic activity and good properties as a mixed ionic electronic conductor (MIEC). While the LSM-YSZ composite demonstrate electrochemical activity mainly in the widened TPB interface, the LSCF has it through the whole cathode due to its good MIEC properties.

Nevertheless, it has been found that insulating phases of $SrZrO_3$ and $La_2Zr_2O_7$ has a tendency to form between the interface of LSCF cathode and the YSZ electrolyte during sintering [14, 20]. GDC and SDC interlayers is often used to inhibit the formation of the insulating phases during sintering. The interlayer also works as a thermal expansion buffer layer between the electrolyte and the cathode, since LSCF has a significantly higher TEC compared to the YSZ electrolyte. Choosing the better LSCF composition would therefore be an influencing factor, since an eventual mismatch can lead to performance degradation during thermal cycles, such as aforementioned delamination [21]. A different approach where nano-sized LSCF particles was prepared by a wet impregnation into a pre-sintered YSZ layer on top of the YSZ electrolyte, created a nano-structured LSCF-YSZ composite cathode. This study showed good performance for the SOFC, with reduced TEC mismatch [3].

2.1.6 Shrinkage

After a tape is casted it will shrink due to drying and sintering, a process that can lead to imperfections. It has been found that cracks usually form under slow drying, when there is a greater water ratio present in the slurry [22]. More water will lead to higher drying shrinkage. This causes the

particles to move a bit while they settle as the water leaves and the tape becomes denser. Different slurry formulations and materials lead to differences in the shrinkage kinetics, thus being an important aspect when the goal e.g. is to co-cast two different slurries [36].

Shrinkage due to densification is by far the biggest contributor to deformation during sintering. The particle size will therefore play a big a role in the densification. Where smaller particles leads to a denser and less porous layer, which means higher shrinkage. And vice a versa. Normally the shrinkage is around 20 - 25 %, but will in the end depend much on the solvent ratio.

2.2 Electrochemical Evaluation

To verify or dispel possible improvements, it is necessary to have the samples undergo different trials and experiments. Through characterizing with the help of recorded results, the samples are feasible to compare against each other.

2.2.1 Voltage-current Characteristics

The characteristic curve, also called polarization curve, is the most common way to study the performance and behavior of a fuel cell. Fuel cell data acquisition can be done three ways, through voltage-, current- or power control. Current- and voltage control is most commonly used. During operation, the cell voltage is altered through a series of values, and for each value the corresponding current values are then recorded. Or the other way around. Afterwards the voltage is plotted against the current density i, where the current density is current divided by the area of the fuel cell (mA cm^{-2}). The use of current density makes the comparison between differently sized fuel cells easier. Figure 2.8 shows a typical characteristic curve.

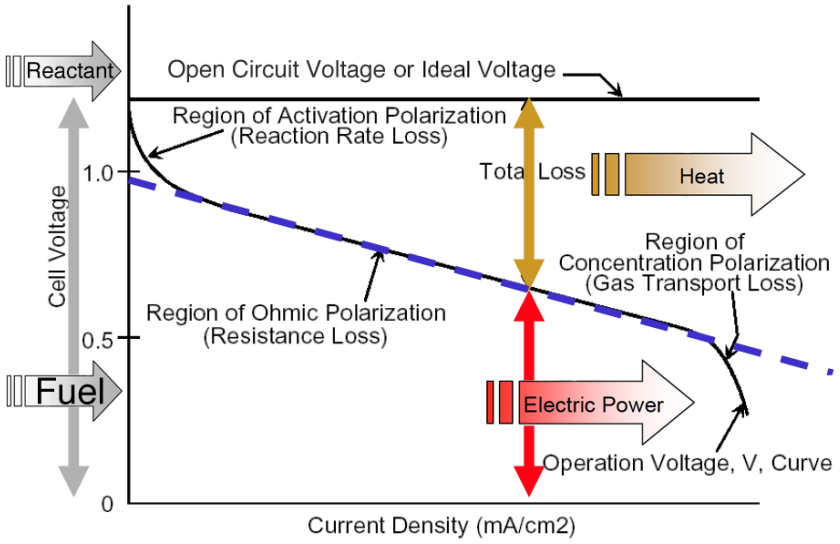

Figure 2.8: Graph showing a typical fuel cell polarization curve [26].

An electrochemical reaction has both a forward and a reverse direction. Take for example the hydrogen reaction, J_1 for the forward direction and J_2 for the reverse. When evaluating the overall rate of reaction $J = J_1 - J_2$, both directions of the reaction has to be considered. Both directions are contributing with current density, forward and reverse. At thermodynamic equilibrium these current densities must balance each other $i_1 = i_2 = j_0$, so there is no current density in sum flowing ($i_1 - i_2 = 0$) in the circuit.

$$Forward\ (Electrolysis): \quad J_1 = H_2 + O^{2-} \rightarrow H_2O + 2e^- \tag{2.9}$$

$$Reverse\ (Fuel\ cell): \quad J_2 = H_2O + 2e^- \rightarrow H_2 + O^{2-} \tag{2.10}$$

On the contrary, even though the sum of reactions are zero, both forward and reverse reactions are taking place.

$$H_2 + O^{2-} \leftrightarrows H_2O + 2e^- \tag{2.11}$$

Where the rate of reactions is distinguished by *exchange* current density j_0, a state that is called dynamic equilibrium [30]. Most often, the potentials (charge transfer) of the forward and reverse reactions may not be equal. If the activation barrier for the reverse direction is much smaller than the activation barrier for the forward reaction, then the reaction rate is much higher for the reverse reaction than the forward.

The open circuit voltage (OCV), also known as the fuel cell potential (dynamic equilibrium), is typical around 1 V for SOFCs. This potential is decreased as a result of various types of irreversible losses, as displayed in Figure 2.8. There are four major irreversibles that is cause to this voltage drop, which are activation losses, fuel crossover losses, ohmic losses and concentration losses. It is mainly these losses that shapes the polarization curve and influences how well the FC perform.

The OCV can be calculated by using the Nernst equation (2.12), as long as the partial pressures for the reactants and fuel is known.

$$E_{OCV} = E^0 - \frac{RT}{nF} \ln \frac{p_M^{v_i} p_N^{v_i}}{p_A^{v_i} p_B^{v_i}} = E^0 - \frac{RT}{nF} \ln \frac{p_{H_2O}^1}{p_{H_2}^1 p_{O_2}^{1/2}} \tag{2.12}$$

Where E^0 is the reversible voltage at standard-state conditions STC, which means that the temperature T is at room temperature (in Kelvin). R is the ideal gas constant, n is number of moles of electrons transferred and F is Faraday's constant. For the log function, reactants are set as denominators and products as numerators. Each reactant and product has its corresponding stoichiometric coefficient v_i. The Nernst equation tells how the reversible OCV changes as a function of different gases concentration and gas pressure [30].

Take for example a H_2 - O_2 SOFC in equilibrium state, at 810 °C. The half-reactions are canceling out each other, so no measurable voltage potential, therefore $E^0 = 0$. For normal conditions, there will be a small amount of unreacted oxygen ions at the anode side, which has a very small partial pressure compared to the hydrogen. Since there are no electrochemical reactions happening, lets rule out the hydrogen and only focus on the oxygen present at both the anode and cathode side. On the cathode side the oxygen has a partial pressure of 0.21 when supplied from air. Now, in order to speed things up the partial pressure at the anode side is reduced to a value of 10^{-20}. Compared, the concentration of oxygen at each side is largely different now. This creates an unbalance, and as a result the difference in concentration will start to equalize, until it reaches balance. Like a pump, oxygen is transfered from the cathode, through the oxygen ionic conducting electrolyte and to the anode side. This transfer can be calculated by the Nernst equation (2.13), a transfer that generates 1.039 V, only driven by concentration difference.

$$E_{OCV} = 0 - \frac{(8.314)(1083.15)}{(4)(96400)} \ln \frac{0.21}{10^{-20}} = -1.039V \tag{2.13}$$

The cell voltage is a sum of the OCV and the irreversible losses as seen in the following equation (2.14).

$$E_{cell} = E_{OCV} - \eta V_{activation} - \eta V_{ohmic} - \eta V_{concentrarion} - \eta V_{crossover} \tag{2.14}$$

1) *Activation losses.* To get electrochemical reaction kinetics going in a given direction, 'reverse' for a FC and 'forward' for an electrolyzer, a prize in voltage loss has to be paid. This voltage loss goes to speed up slow reaction kinetics and low catalyst activity, which is happening on the surface of the electrodes. The effects of the loss is most often experienced to be at low current densities, as can be seen in Figure 2.8 where the voltage drop is highly non-linear. In order to minimize activation losses, the catalyst area must be highly utilized and the catalyst activity improved. Other measures can be increased cell temperature, increased reactant concentration or increased pressure.

2) *Fuel crossover losses and internal currents.* When the thickness of the electrolyte is decreased, the crossover of fuel from the anode to cathode side may increase, but depends on electrolyte density. The result of this fuel crossover causes electron conduction through the electrolyte, which creates an internal current. Ions should be the only thing transporf across the electrolyte, but as it is, there will always be a possibility for these losses. However, these effects has been found to have bigger impact on low temperature fuel cells than SOFC.

3) *Ohmic losses.* One of the reasons to reduce the electrolyte thickness, would be to decrease the ohmic losses, since its ionic resistance is one of the main contributors to it. In addition, electronic resistance from the electrodes and their external connecting circuit and contact resistance adds to the equation. In fuel cell stacks, various interconnections would also contribute resistively. This voltage drop is usual proportional to the current density, in other words linear as displayed in Figure 2.8. A way to determine the ohmic resistance in the fuel cell, is by use of EIS.

4) *Concentration losses.* Or mass transfer loss, is caused by changes in the concentration of the reactant. As the result of doubling the reactant concentration can increase the FC performance, the opposite is the case in this situation. Reduction of concentration, is the consequence of the inability of the FC system to transport enough reactants to the electrode surface as the fuel is being used. Which gives reason to why it is also called mass transfer loss. The occurrence of these losses, where the characterization curve bends down at the end, would normally mark the operational limit of the fuel cell [18, Ch.3] [30] [40, Ch.21].

Multiplying current density with the voltage, gives power density and then as illustrated in Figure 2.9 the power curve is plotted versus the current in the same graph as the IV curve. This additional curve can show where the maximum power point (MPP) is to be located along the characteristic curve. In other words, at which point the fuel cell operates most efficient and generates maximum electrical power.

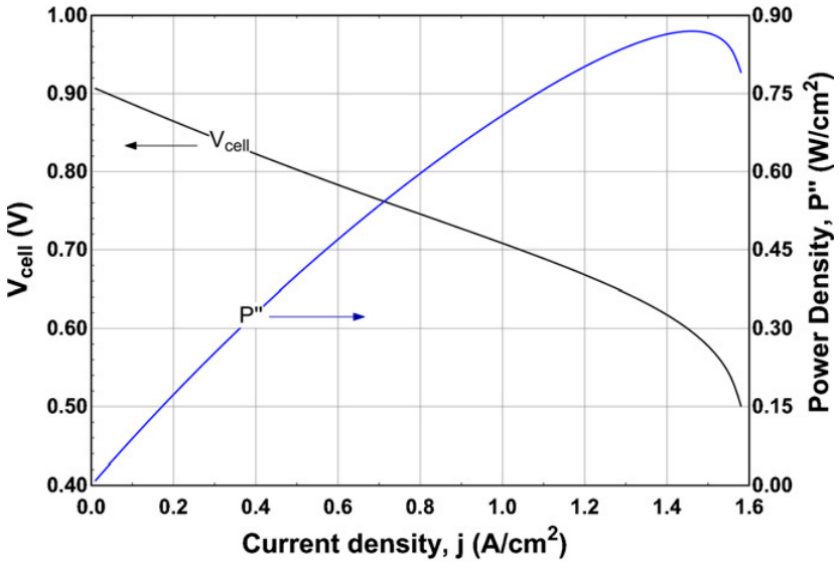

Figure 2.9: SOFC polarization curve and power density. [1]

The SOFC is often called a thermally activated process, it needs to surpass an activation barrier (*activation losses*) to make the electrochemical reactions occur. When the activating amount of energy (commonly known as activation energy) is reached, it will set the electrochemical reactions in 'reverse' motion, creating a current. By providing more thermal energy, it will lower the activation energy and thus the voltage loss too. Causing the reactions to happen much faster and more easily. The process' thermal dependency can be described by the Arrhenius equation.

Arrhenius' equation gives the temperature dependent rate constant σ, of a chemical reaction, with respect to the absolute temperature T, given in Kelvin. In this case σ is also the same as conductivity. σ_0 is the pre-exponential factor, a constant. E_A is the activation energy and R the universal gas constant (8.314 $JK^{-1}mol^{-1}$).

$$\sigma = \sigma_0 \exp\left(\frac{-E_A}{RT}\right) \tag{2.15}$$

By applying the log function to the equation, it can be altered into a more intelligible expression, which then resembles a linear equation.

$$\ln(\sigma) = \left(\frac{-E_A}{R}\right)\left(\frac{1}{T}\right) + \ln(\sigma_0) \tag{2.16}$$

$$y = ax + b$$

Where $ln(\sigma)$ is the equations y, and $1/T$ is the x. The slope (a) of the line is $-E_A/R$ in

Kelvin, and $\ln(\sigma_0)$ is (b) the y-axis intersection. The Arrhenius plot is made by plotting $\ln(\sigma T)$ as a function of $1/T$. Plot data can be acquired through SOFC single cell experiments in the laboratory. Where the conductivity of the object and absolute temperature is measured over a range of temperatures, e.g. from 900 to 1200 K. The conductivity is calculated by:

$$\sigma = \frac{(I/A)L}{U} \tag{2.17}$$

Where I is the current measured, A is the area of the sample, L is the thickness of the sample and U the measured voltage. By using line regression on the experiment data, $ln(\sigma T)$ and $10^4/T$, the linear equation 2.16 can be found. Afterwards the activation energy is calculated from the slope value 2.18, and lastly the pre-exponential factor 2.19.

$$a = \frac{-E_A}{R} = slope \;\; \Rightarrow \;\; E_A = -aR\,[kJ\ mol^{-1}] \tag{2.18}$$

$$b = \ln(\sigma_0) \;\; \Rightarrow \;\; \sigma_0 = \exp(b)\,[S\ cm^{-1}] \tag{2.19}$$

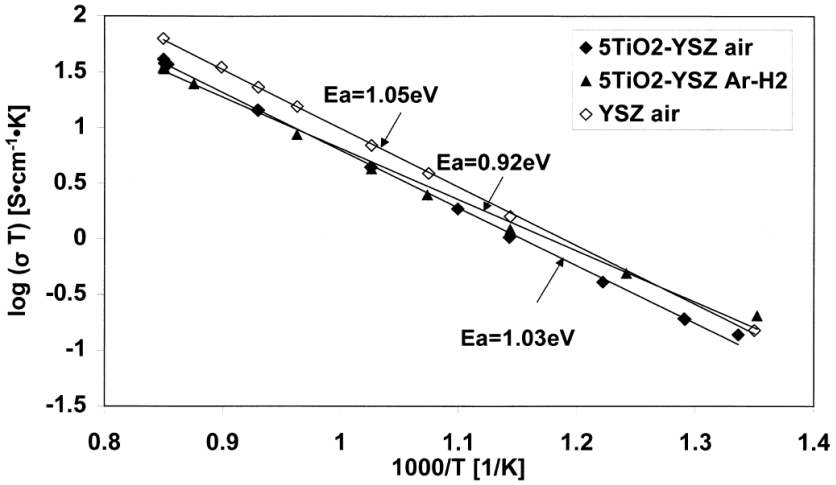

Figure 2.10: Arrhenius plots of total electrical conductivity for YSZ in air and 5TiO_2-YSZ in air and Ar-4% H_2 [35].

Obtaining the activation energy of a sample is helpful when validating whether it performs better or worse. A lower activation energy would indicate a better cell potential, which could mean higher FC efficiency as temperature continues to rise.

As shortly and indirectly mentioned in the beginning of this section, the activation barrier (energy) can be reduced. This can be done by altering the electrode reaction rates, which can be altered through measures already mentioned in the paragraph of *Activation losses*. Figure 2.11 shows the energy changes in the cathode exemplified, where the yellow line shows the system at equilibrium state. Changing the potential of the electron energy (red arrow), decreases activation energy (blue arrow), and leads to an increased reaction rate in reverse direction (white dashed line). By inducing a faster electrode reaction rate (large exchange current density), a smaller over potential (activation energy) are needed to set things in motion. While slower electrode reactions (small exchange current density) will require a large over potential (activation energy).

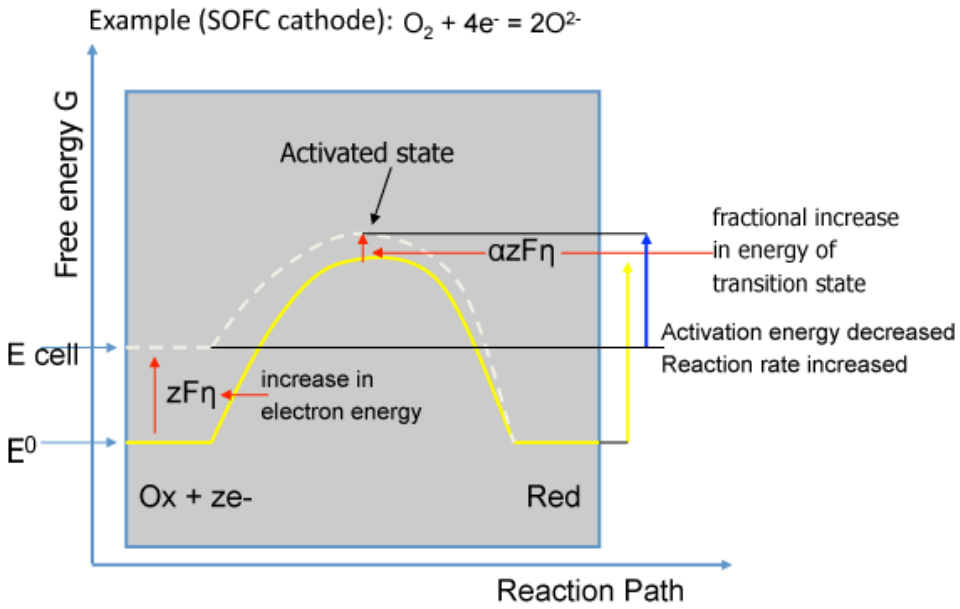

Figure 2.11: Cathode electron transfer energy diagram: $O_x + ze^- =$ Red [27].

Both electrodes contributes to the total activation energy. The hydrogen oxidation reaction (HOR) is rather simple compared to a more complex ORR, which is why it is much faster. Put in contrast, the HOR kinetics are very fast, whereas the ORR is very slow. For this reason, the majority of the voltage loss draws to the cathode side (needs more activation energy), where the ORR happens. For a simplified illustration, Figure 2.12 shows the correlation between the exchange current density size and the activation energy. A larger exchange current density yields lesser voltage loss.

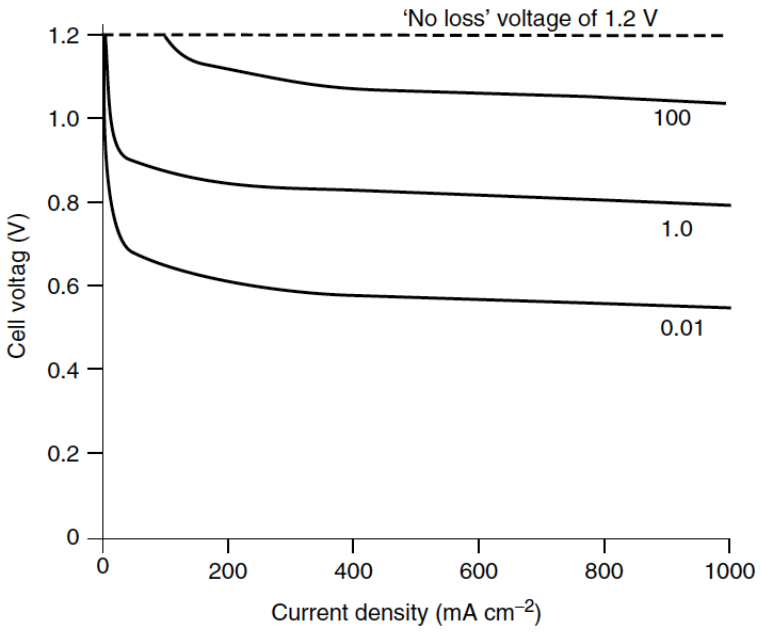

Figure 2.12: Graphs of cell voltage against current density, assuming losses are due only to the activation energy at one electrode, for exchange current density j_0 values of 0.01, 1.0, and 100 mA cm^{-2}. [18, Ch.3].

The Butler-Volmer equation (2.21) is stricly valid for single- or a few electron transfer events. However, together with an example plot, it still helps to illustrate the electrochemical reaction and wrap together a few of the terms spoken of here. The equation (2.21) consists of two parts, the anodic and the cathodic, where each part is represented separately in Figure 2.13.

$$i_{total} = j_0(i_{anode} - i_{cathode}) \tag{2.20}$$

$$i_{total} = j_0(\exp\left(\frac{\alpha n F \eta}{RT}\right) - \exp\left(\frac{-(1-\alpha) n F \eta}{RT}\right)) \tag{2.21}$$

Where $\eta = E_{cell} - E^0$ is the over-potential or activation over-voltage (see Figure 2.11), α the charge transfer coefficient (symmetry factor), n is the number of electrons, F is the Faraday constant ($9.6484 \cdot 10^4\ C\ mol^{-1}$), R is the gas constant ($8.314\ J\ mol\ K^-1$) and T the absolute temperature in Kelvin.

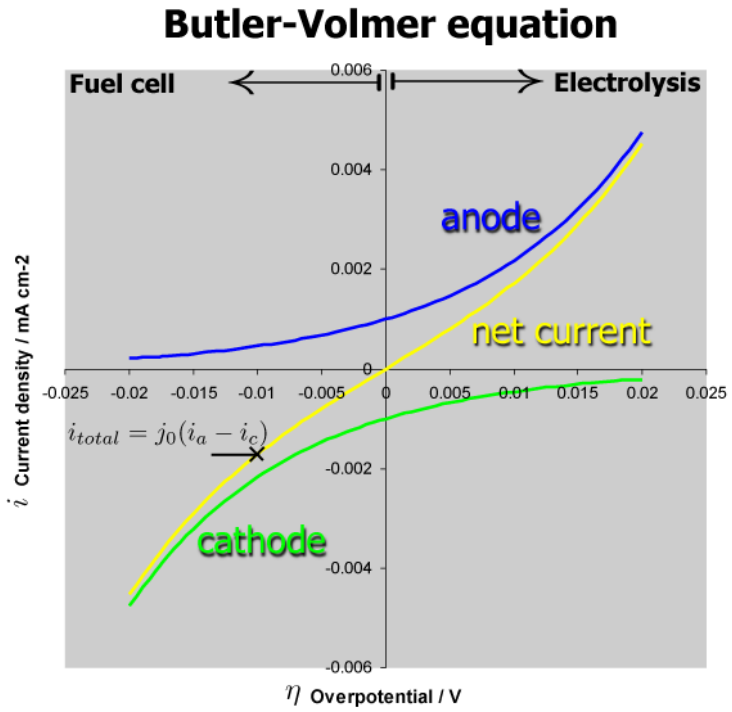

Figure 2.13: Charge Transfer Kinetics between the anode and cathode, here with symmetric reactions ($\alpha = 0.5$) [27].

Figure 2.13 shows a symmetric case, where the anode and cathode contributions cancel each other out at (0,0). Which is the point at where the system will be in dynamic equilibrium. The electrochemical reactions exchanging both forward and backwards at the same time. The sum of the electrode contributions is represented as the net current. With negative (drawing) over-potential the electrochemical reaction is set in reverse direction, behaving as a FC. With positive (applying) over-potential the reaction is set in forward direction and the system behaves as an electrolyzer. As soon as the system is set in e.g. reverse reaction, the net current (density) will begin to flow. Simplified, the current density is the sum of the currents from each electrode. For an asymmetric case, which is more common, it would require less activation energy to set the system in one direction, compared to the other.

2.2.2 Electrochemical Impedance Spectroscopy

Electrochemical impedance spectroscopy (EIS), also known as AC impedance testing, is a non-destructive evaluation method. It can provide time dependent information about a system's or subject's condition during normal operation or testing. It is used for both diagnostic (e.g. degradation, quality control) and application (e.g. system optimization, -controlling) purposes. The data is interpreted and analyzed through various methods, and are presented in diagrams. It is a helpful

method to break down the total FC impedance into the contributions of the different components and processes in the cell. In order to interpret the data it is necessary to make a good curve fitting and equivalent circuit model.

An operating fuel cell generates DC current, and the way AC impedance spectroscopy works, is by superimposing a small AC current signal to the DC current going through the electrodes, expressed as a function of time.

$$i = \hat{i} \sin(\omega t) \tag{2.22}$$

Where i is the instantaneous current, $\hat{i}$ is the current amplitude, and ω is the angular frequency in (in $rad\ s^{-1}$), also known as $2\pi f$. The measured response signal is a phase sensitive AC voltage, with a different amplitude and phase (ϕ).

$$u = \hat{u} \sin(\omega t + \phi) \tag{2.23}$$

Where u is the instantaneous voltage, $\hat{u}$ is the voltage amplitude, and ϕ is the phase shift. By using Ohm's Law, the following expression is used to calculate the impedance, expressed as a magnitude z, with the phase shift ϕ.

$$Z = \frac{u}{i} = \frac{\hat{u} \sin(\omega t + \phi)}{\hat{i} \sin(\omega t)} = z \frac{\sin(\omega t + \phi)}{\sin(\omega t)} \tag{2.24}$$

On the other hand, by using Euler's relationship,

$$\exp(j\phi) = \cos(\phi) + j \sin(\phi) \tag{2.25}$$

the impedance is possible to express as a complex function, by describing the superimposed current as,

$$i = \hat{i} \exp(j\omega t) \tag{2.26}$$

and the voltage response as,

$$i = \hat{i} \exp(j\omega t - \phi) \tag{2.27}$$

The impedance can then be expressed as a complex quantity [10],

$$Z(\omega) = \frac{u}{i} = z\exp(j\phi) = z(\cos(\phi) + j\sin(\phi)) = Z_{Re} + Z_{Im} \tag{2.28}$$

AC impedance testing is performed at as stable conditions as possible, fixed temperature, fixed partial gas pressures and with a fixed load. Each test is done while the cell is operating at a specific point on the IV- curve. The AC voltage amplitude and phase are measured during a frequency sweep, typical in the range of 10 µHz to as high as 1 MHz. The result after being calculated is a full impedance spectrum. Multiple tests along the IV-curve can be performed in order to link fuel cell processes and properties to the properties of the impedance spectra. For example perform tests in the activation losses domain, in the ohmic domain and where the concentration losses are located, as illustrated in Figure 2.1.

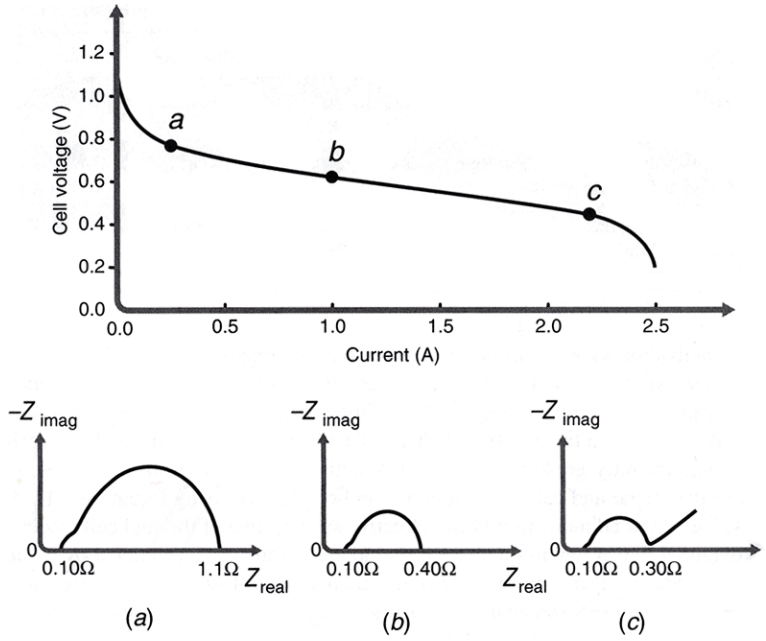

Figure 2.14: EIS characterzation of a due cell requires impedance measurements at several different points along an I-V curve. The impedance response will change depending on the operating voltage. (a) At low current, the activation kinetics dominate. (b) At intermediate current (higher activation over voltages), the activation loops decrease. (c) At high current, the activation loops may continue to decrease, while the mass transport effects begin to intercede, resulting in the diagonal response at low frequency [30].

Since impedance is a complex quantity with both a real, Z_{Re}, and a imaginary component, Z_{Im}, EIS data are generally represented in Bode and Nyquist plots. In a Nyquist plot the Z_{Re} is plotted along the x-axis and the Z_{Im} along the y-axis, as illustrated in Figure 2.15. Since the SOFC Z_{Im} component in sum is most often capacitive, the y-axis is inverted with the negative side up for practical reasons. Every point on this half circle curve is the impedance value at one frequency.

The impedance can be presented as a vector of length $|Z|$, where the angle between the vector and the x-axis is $\phi = (argZ)$, as illustrated in Figure 2.15. Still the downside with the Nyquist plot is that you can not read from it what the frequency for a given point is, but it is possible to calculate it if the complete data information is available [9].

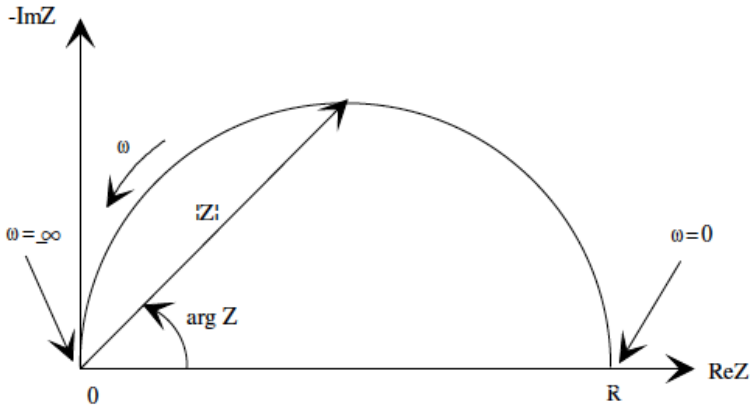

Figure 2.15: Nyquist plot with impedance vector [9].

From the recorded impedance spectra it is possible to calculate fuel cell parameters either by hand or with the aid of a EI spectrum analyzing program. The process is complex and the pitfalls are many. When parameters has been found they are normally fitted to an electrical equivalent circuit model (ECM), with the use of basic electronic components such as resistors, conductors and inductors with grouping of parallel and series combinations.

An example circuit is shown in Figure 2.16. These ECMs are used to interpret the test results linked to the cell properties, and can either be made simple or complex depending on what the purpose might be. The goal of the circuit can be to replicate the behavior of the fuel cell, so that it for example can reproduce the I-V curve. Other aspects of the fuel cell such as changes in gas partial pressures can also be included [31]. For making a functional computer simulation of a real single cell or system, model fitting of impedance spectra would be included as an important tool.

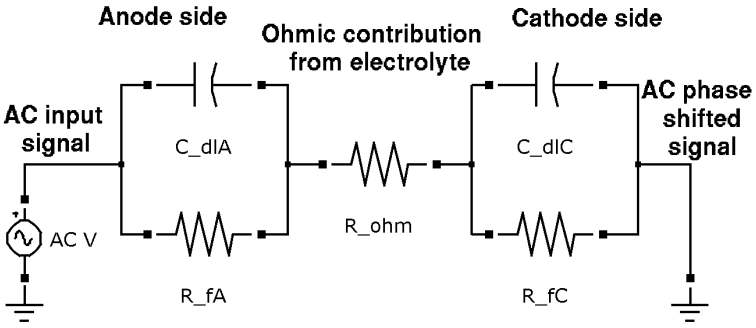

Figure 2.16: Equivalent circuit model example which is the basic model of any electrochemical cell.

For the Bode plot there is usually two plots together. The impedance is plotted with log of frequency for both on the x-axis, where the absolute values ($|Z|=Z_0$) of the impedance are on the y-axis for one plot and the phase shift for the second plot. Compared to the Nyquist plot, the Bode plot show the frequency information. An example plot is illustrated in Figure 2.17 [9].

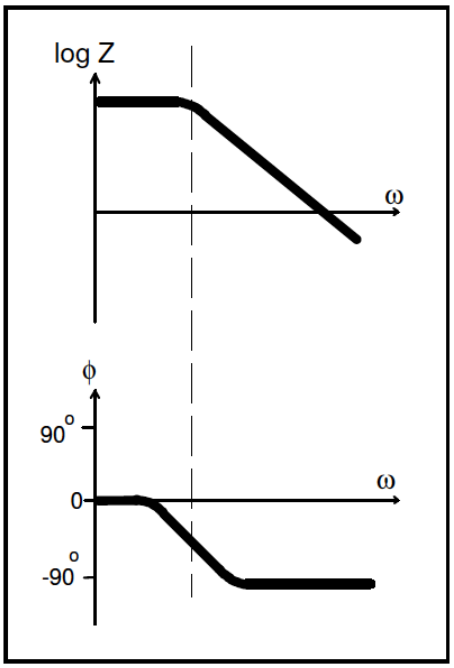

Figure 2.17: Bode plot [9].

Chapter 3

Method

This chapter introduces the methodology consisting of the practical tasks, the setup of each process and execution of these. Starting with a description of the creative process for producing a self-made tool, continuing with the stepwise production process of substrates, micro-structural analysis, electrochemical evaluation and lastly thermal and redox cycling.

3.1 Making of Adjustable Tape Casting Device

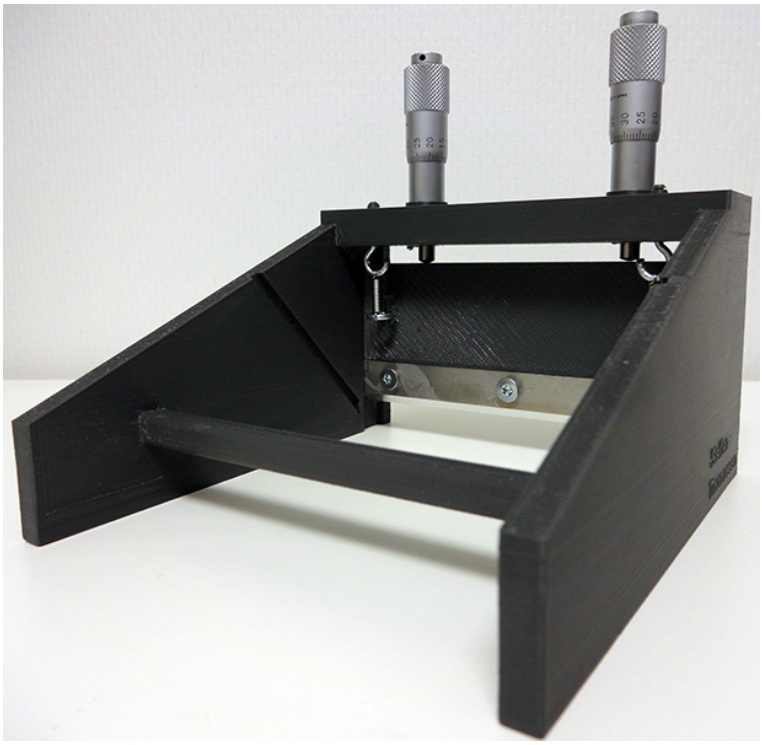

Figure 3.1: Completely assembled model.

In order to reach the objectives of the project it was necessary to make a tape casting system, making it possible to produce SOFC thin films (substrates). After some researching, the approach to the production was clarified. The main parts were directly made, designed and 3D-modeled in Autocad and 3D-printed at a facility at the University of Agder. An aluminum blade profile was produced by CNC-milling in the University workshop and the rest of the parts were ordered.

3.1.1 Requirements

The tape casting device should be adjustable and precise enough to cast a uniform 1 mm slurry with a 0.1 mm accuracy. The chosen Mitutoyo micrometer heads has a 0.01 mm precision, which should be more than sufficient to satisfy the models accuracy criteria. The complete constructed model will quickly show how precise a mix of 3D-printed, CNC-cut and ordered parts can perform together, making this is a small project in itself. Apart from these requirements, the tape caster should be easy to use and adequately sturdy for its application.

3.1.2 Design Specification

The tape casting device as shown in Figure 3.2, consists of the main body structure with two incorporated slots. The main slot is placed underneath the mainstay of the body, and contains a vertically oriented, rectangular carrier plate which also contains a slot. This slot houses an aluminum doctor blade, which is fixed to the carrier plate by three screws. Second slot is designed for a guide plate that tilts downward towards the carrier plate. Two eyebolts are connected underneath the mainstay, to the inside of the carrier plate, on each side. Aligned directly above these, an additional pair of eyebolts is connected to the mainstay. On each side, a tension spring will be connected between the eyebolts of the carrier plate to the eyebolts of the mainstay, two springs in total. Above on the mainstay, directly above the vertical carrier plate, there are two slot holes. These holes hold one micrometer head (see Figure 4.1) each, where a locking nut shall be attached to them underneath and between the mainstay and carrier plate. That would be the total model. An illustration of the model is shown in Figure 3.2.

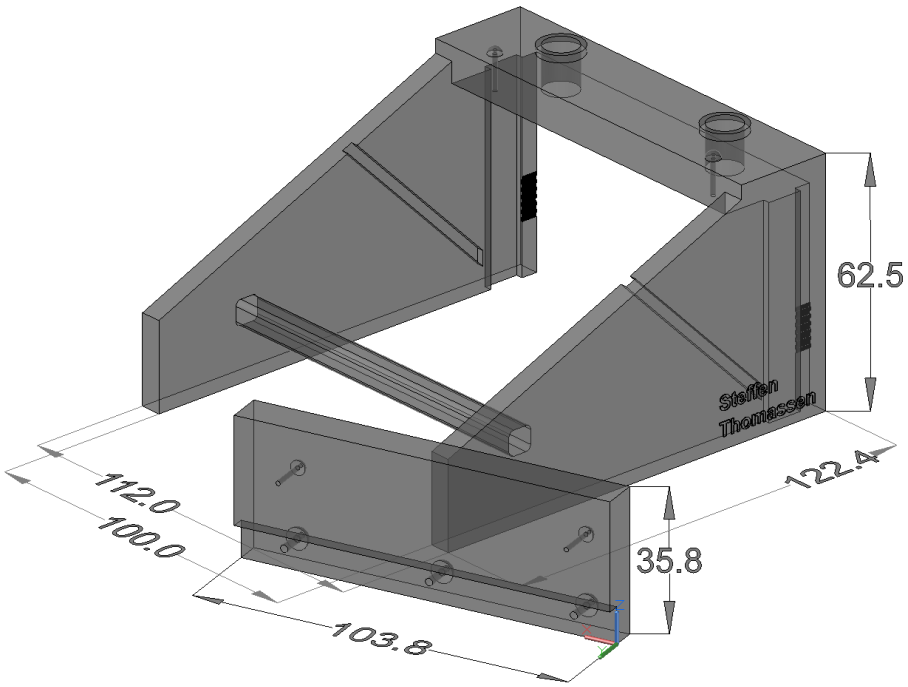

Figure 3.2: Final AutoCAD model ready for 3D-print, without guide plate. Dimensions are in mm.

When connected, the tension springs will hold the carrier plate in place. To adjust the doctor blade closer to the ground surface, the micrometer tips are extended to work against the springs and press the blade down. This force-counterforce put on the carrier plate will stabilize the construction, as shown in Figure 3.3. Compression springs were first considered, but since it would pose a problem on how to retract the carrier plate with the micrometer tips, tension springs was the practical choice.

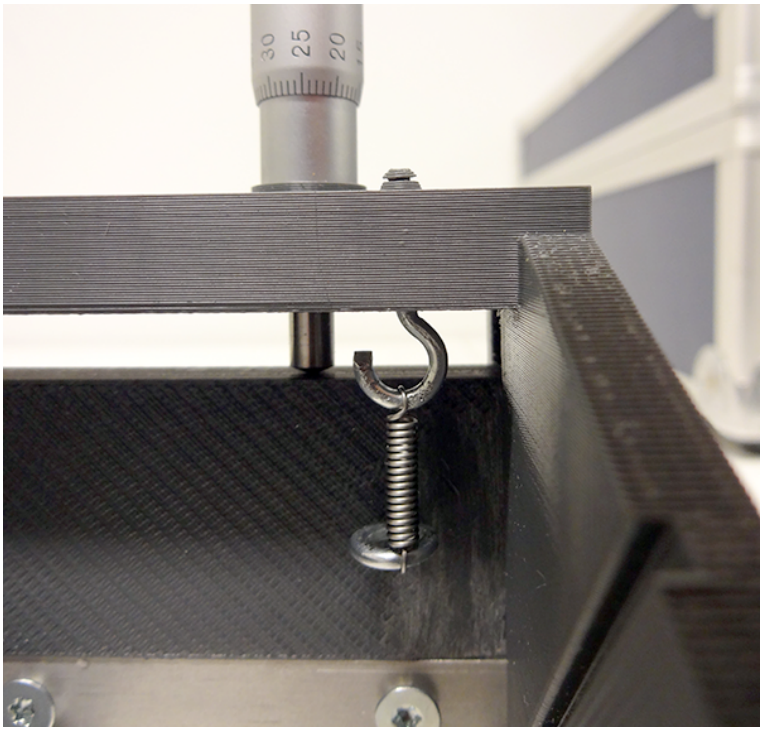

Figure 3.3: Micrometer tip against counter-force from the spring.

1x1x1 cm test cubes with a 1 mm hole throughout were printed, where the hole had z-axis orientation. Since the printer builds layer by layer in the xy-plane, the hole pierced every layer. Steel bolts with somewhat larger diameter than the hole were screwed into the cubes, to evaluate the strain it could impose. To put things short, the screws gave in before the test cubes did. Nevertheless, after a few days the cubes showed sign of cracks. As a result the screw holes for the model design were widened with 0.3 mm and also oriented as best could. Had the hole been oriented along the xy-plane, the screw would simply work as a wedge between two layers, and thus break them apart.

The carrier plate, as well as the guide plate was printed flat down, so that the build layers would have the correct orientation. The model has been designed to work together with a 6.67 mm thick laminated glass plate with dimensions 99.5 mm x700 mm. With the tape caster put above the glass plate, the walls of the tape caster will function as guiders along the outside of the glass plate, as shown in Figure 3.4. As a choice the guide plate can be used to pour the slurry directly against the doctor blade, if not, the slurry is put on to the glass plate and the tape caster is in the end pushed slowly and steady along the glass plate.

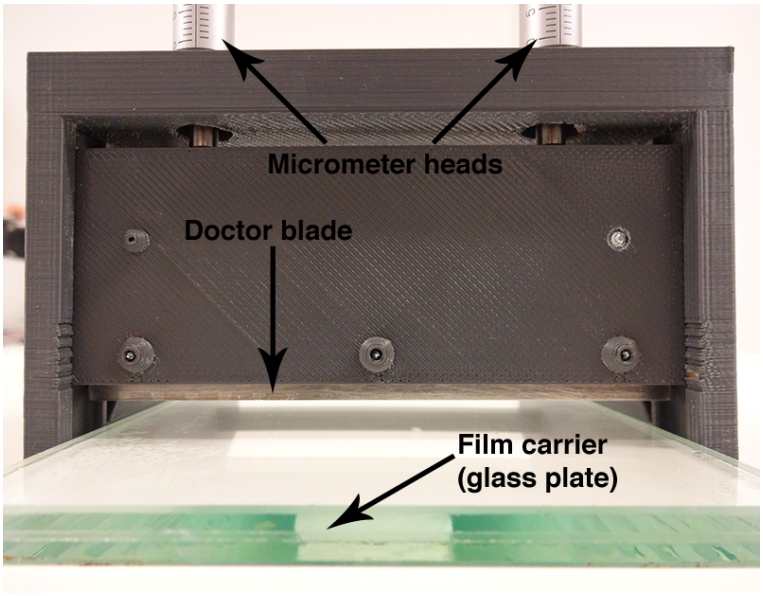

Figure 3.4: Tape casting device set up together with the glass plate.

3.2 Equipment and Production

When tape casting, the slurry must be adjusted so that the resulting tapes fulfill some quality criteria, as follows:

1) No defects during drying.
2) Flexible and good self-bonding to allow shaping and manipulation of dried films.
3) Micro structural uniformity.
4) Good lamination ability, for multiple layer casting.
5) Easy burnout of solvent, plasticizer and disperser.
6) High mechanical strength after sintering, which includes any supporting layer.

In order to reach these criteria, it is important to choose good materials and at the same time having good control of several processing parameters [7]. All materials were ordered from Sigma-Aldrich.

3.2.1 Experimental Mixing and Milling

To conserve materials, small batches were put in small bottles and put in a bigger container to use the ball-milling machine. The recipes for making the tape cast slurries are based on a standard recipe used in other projects, which I received from my supervisor. The project recipes has been experimentally found, as each slurry needs optimization. A picture of the ball-milling setup is shown in Figure 3.5. Zirconia grinding medium in the form of balls are used to mill the slurry and disperse agglomerations. Spot checks were performed during slurry composing to quickly determine if the slurry had undesirable traits, both before and after a period of ball-milling. A small amount of slurry was spread across a microscope slide, where it dried for some time. The sample was studied in an optical microscope to check agglomeration behavior. Afterwards the samples was tried peeled of the glass slide to test self-binding and flexibility properties.

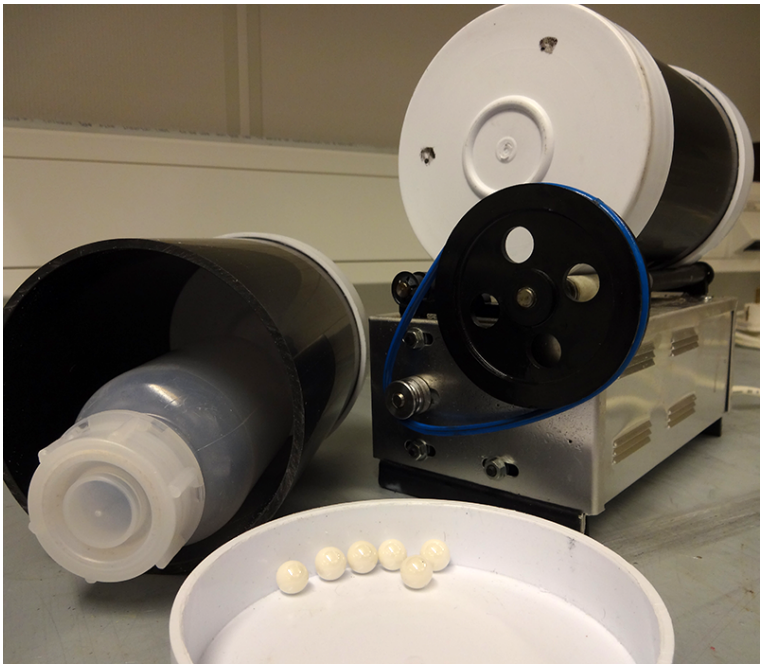

Figure 3.5: Ball-milling equipment and setup.

Table 3.1: Binder formula for both 20% and 30% concentration

Ingredient	**Description**	**Ratio**
Binder	PVA (polyvinyl alcohol)	0.2/0.3
Solvent	Distilled water	0.8/0.7
Total		1

Binder was made by the ratios 20/80 and 30/70 of PVA and distilled water. The mix was put in a glass container and heated close to boiling point while stirred, until the PVA was completely dissolved. Binder is used in all of the slurry recipes.

Table 3.2: YSZ-electrolyte formula

Ingredient	**Description**	**Weight (g)**
Powder	YSZ	10.15
Solvent	Distilled water	5.85
Binder	PVA (polyvinyl alcohol) 20%	10
Plasticizer	Glyserol	3.15
Dispersant	Tween 80	0.7
Total		29.85

YSZ-electrolyte slurry was composed of 8YSZ powder, binder and an distilled water. After being ball-milled for 2 days, a sample was smeared on a microscope slide and left to dry until next day. The sample turned out too brittle, so an amount of plasticizer was added to the mixture and a new test was spread on the glass slide. The second sample turned out flexible and released easily from the glass slide. The slurry was ball-milled for 14 days. For the electrolyte, it is desirable with as small particles as possible to produce a dense solid layer.

Table 3.3: Titania batch formula

Ingredient	**Description**	**Weight (g)**
Powder	Titania	10
Solvent	Propanol	10.4
Solvent	Distilled water	17.4
Binder	PVA (polyvinyl alcohol) 20%	8
Plasticizer	Glyserol	1.7
Dispersant	Tween 80	0.9
Defoamer	Aceton	9.9
Total		58.3

Since titania was an unfamiliar material to work with, it was necessary to explore the rheology of it when dissolved and mixed with additives. When dissolved with ≤ 20 % distilled water, titania showed non-newtonian properties. A behavior that can pose a problem to the ball-millig process. The non-newtonian behavior could slow down the balls, which would reduce the impact of the milling. By adding more water, a share of Propanol (alcohol with low vaporization rate) and some Aceton (an alcohol with a high vaporization rate), these unwanted properties was eliminated.

Table 3.4: NiO-YSZ cermet formula

Ingredient	Description	Weight (g)
Powder	NiO-YSZ	5
Binder	PVA (polyvinyl alcohol) 30%	3.5
Solvent	-	-
Plasticizer	Glyserol	1
Dispersant	Tween 80	0.4
Total		9.9

The NiO-YSZ cermet is meant to be the supporting layer of the SOFC single cell, which requires the tape casted film to be considerable thicker compared to the other SOFC components. Because of this, it is desirable to have a more viscous slurry. So that it will keep together in a thick layer after casting, instead of flowing outwards while drying. As a result of this, it was necessary to remove the pure water and base the recipe on the water already present in the binder. In addition, a binder with less water was produced for this single recipe.

Before the slurry can be used, it should be vacuumized. This process is performed to remove any air bubbles and foam the slurry may contain. If the bubbles do not burst easily while the air expands under vacuum and just continues to grow, it could be necessary to increase the amount of defoamer or worse, change the solvent medium. For this project a small vacuum chamber was used, as shown in FIgure 3.6, which was operated by a small pump connected to and solely driven by running tap water.

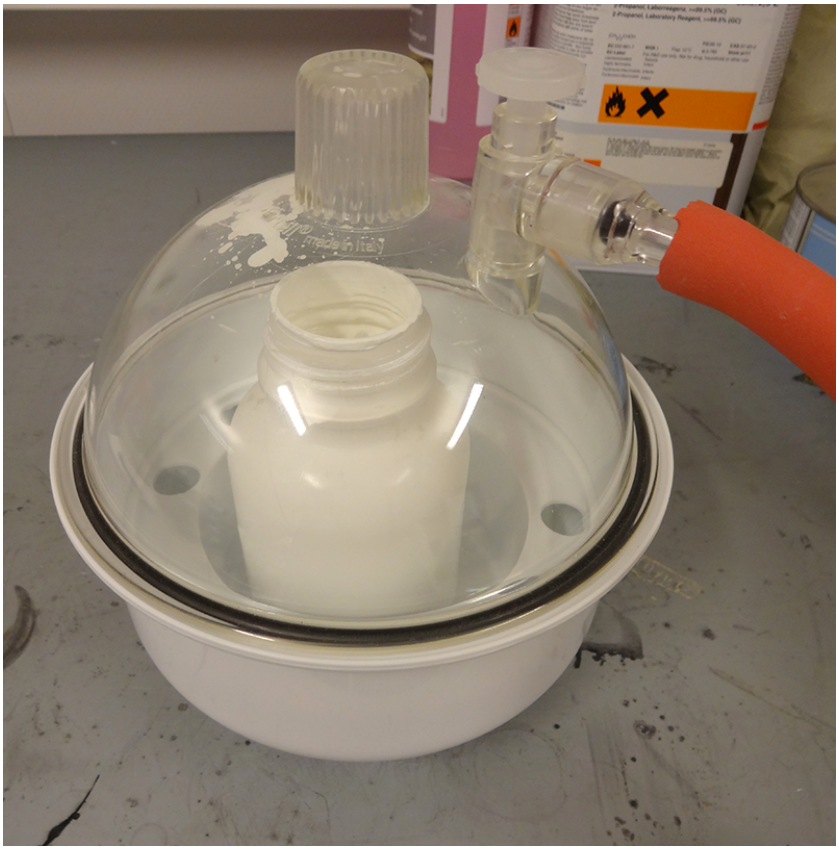

Figure 3.6: Small laboratory vacuum chamber.

3.2.2 Tape Casting and Drying

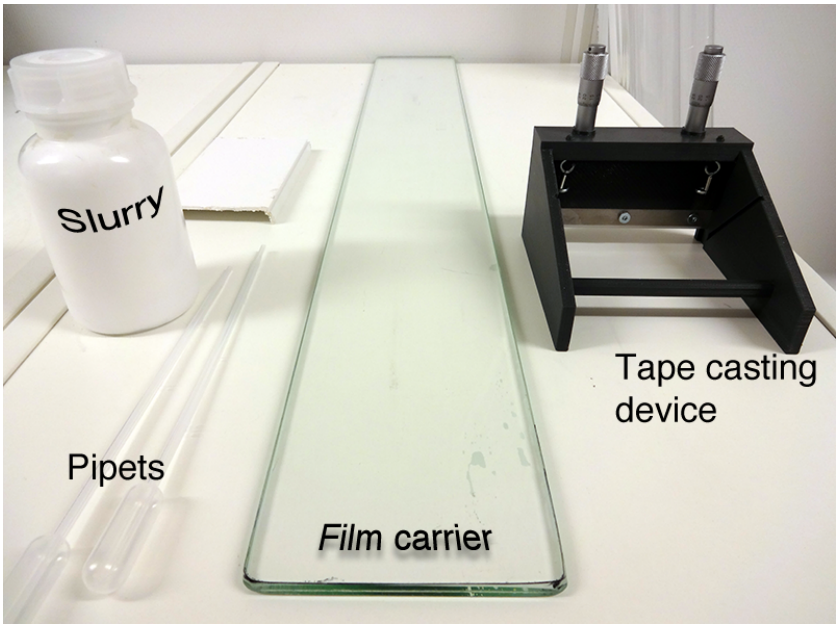

Figure 3.7: Equipment needed. Vacuumized slurry, some pipets, the tape casting device and tailored glass plate (film carrier).

The tape casting device was used to produce thin films, both single and co-casted (two layers). To prepare for tape casting, the equipment in Figure 3.7 is needed, afterwards the tape caster is put above the film carrier and adjusted to the desired gap size.

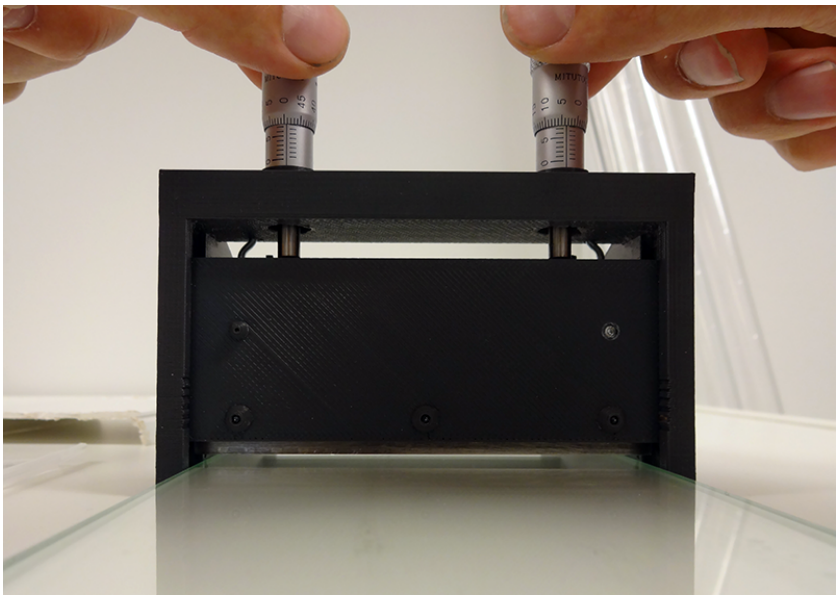

Figure 3.8: Adjusting the gap between the glass plate and doctor blade.

An amount of electrolyte slurry is put on the film carrier,

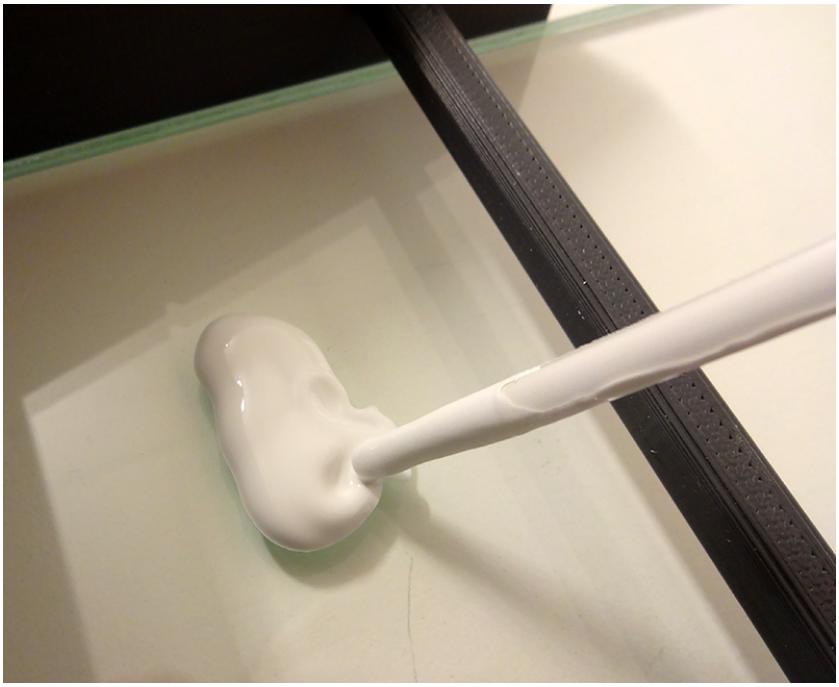

Figure 3.9: By keeping the pipet a bit above the slurry will reduce the chance of blowing air into it.

where it is uniformly distributed into a (close to) 50 µm thin layer.

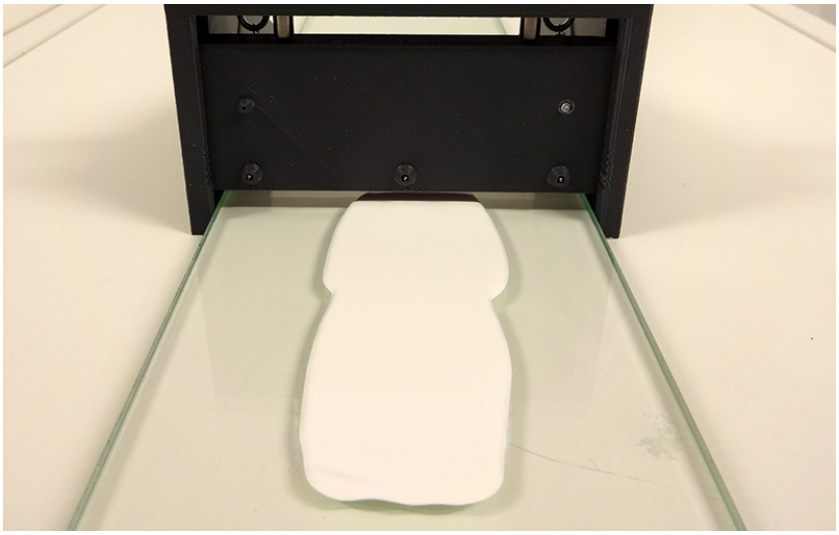

Figure 3.10: Electrolyte evenly spread after two depositions and drags to extend the film a bit.

After one minute an amount of anode slurry can be laid on top, which is then distributed in a 1 mm thick layer across the electrolyte with the tape caster. The result is a co-casted anode and electrolyte film. The layers are left to dry until next day, when it is possible to peel them of the glass plate.

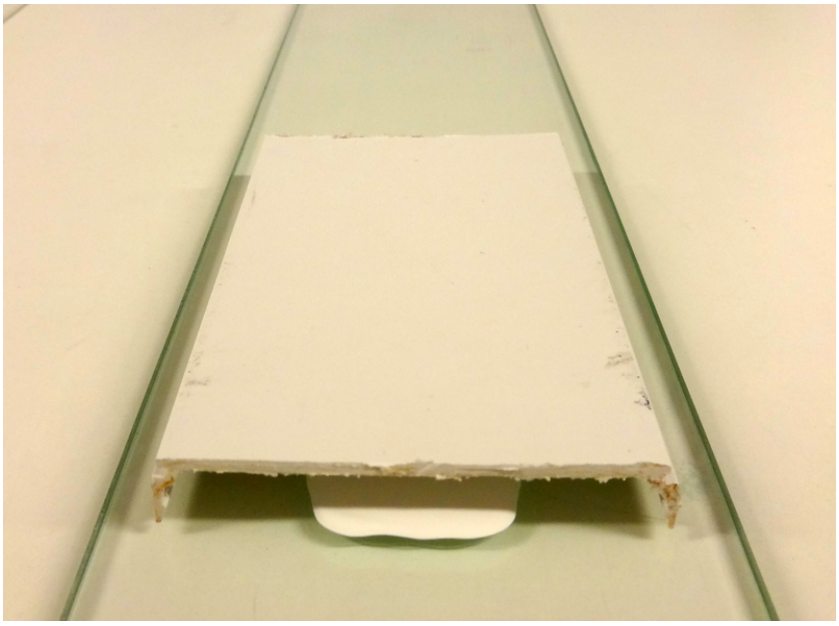

Figure 3.11: It is Important to cover the tape to avoid dust and particles to stick to it.

A more thorough explanation and step-wise guide to the tape casting process is found in Appendix A: Tape casting guide.

A cathode layer is deposited on the sintered co-casted anode-electrolyte layer either by screen printing or just by painting it on. As the cathode components requires a relatively lower sintering temperature than the co-cast layer, it is enough to let the cathode layer dry and let it sinter at the heat levels during operation in the test furnace setup.

3.2.3 Shaping, Burnout and Sintering

The tape samples (films) were cut into square dimensions of 2x2 or 3x3 cm^2. A pair of 10 x 10 cm^2 alumina plates was used as support plates, since the samples could damage the furnace floor. Support plates should be smooth and without any roughnesses that can generate unwanted friction during sintering, which can hinder shrinkage [36]. At first some scrap custom made ceramic plates was used, but the plates showed sign of reactivity towards NiO-YSZ samples. After a few test runs they were damaged by the high temperatures, which is why they were replaced by the alumina plates. To counter eventual reactivity, a thin, flat powder bed of the same sample material was put between the sample and the support plates as shown to the right in Figure 3.12.

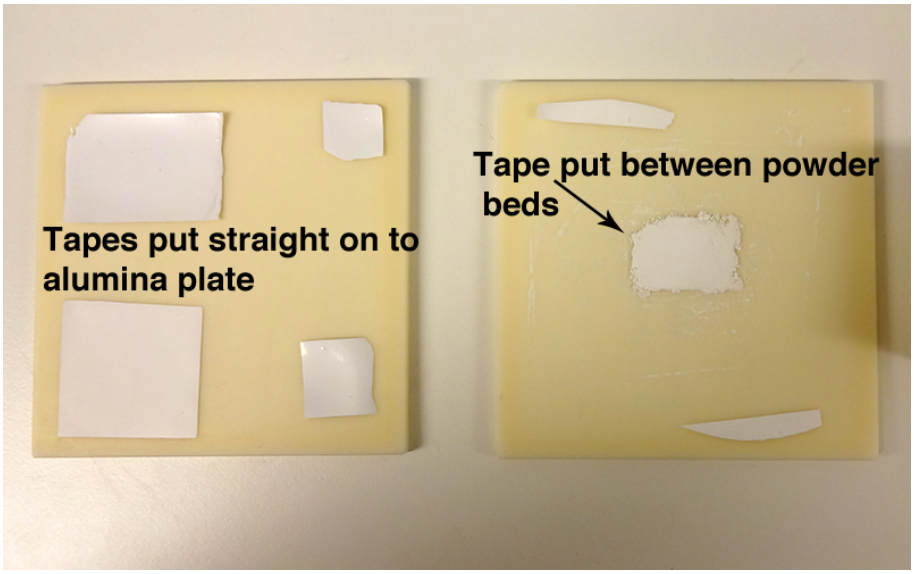

Figure 3.12: Alumina plates with samples prepared for sintering. The sample in the middle of the right plate, was put between powder beds to keep it flat and inert to the plates.

The furnace being used is a Carbolite muffle furnace with silicon carbide heating elements, as pictured in Figure 3.13. Having a 3 liter chamber gives room to stack several support plates with samples every run, which is practical since every run takes about 24 hours total.

Figure 3.13: Sintering furnace, Carbolite, model RHF 16/3.

It is possible to program the furnace, so that a sequence of different temperature plateaus with transitional ramping rates between, can be set. An illustration of the sintering program used in the project shown in Figure 3.14, where the top value is the only experimental and changing value, between 1300 - 1400 °C.

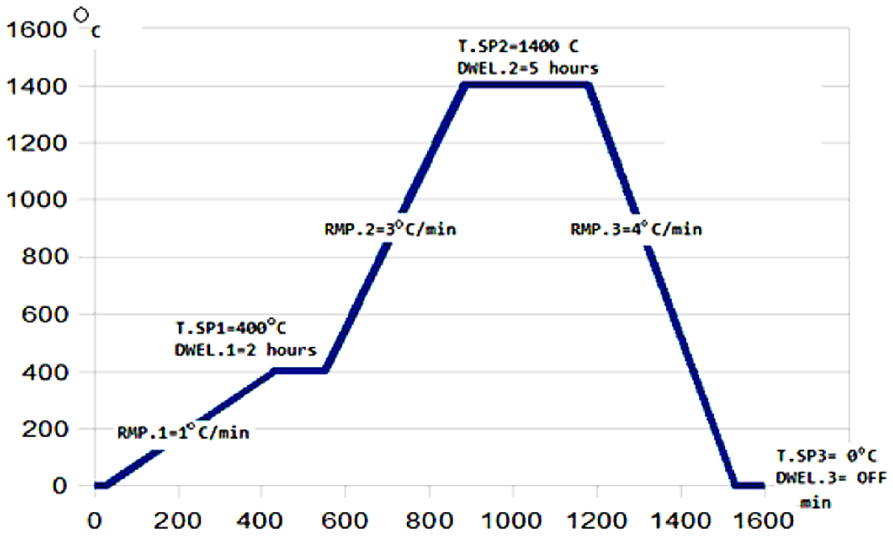

Figure 3.14: Sintering program with different plateaus, with a burnout part followed by sintering, ending with cool down [27].

Before reaching the sintering process the tapes goes through a pre-process called burnout. After slowly ramping up the temperature, the furnace dwells at 400 °C for 2 hours. This is done to get rid of residual humidity, and burn out the binder, plasticizer and disperser in the tape before sintering it at 1300 °C. Burnout prevents cracking in the tape at higher temperatures, that would come from the rapid gas expansion of the additives as they leave (in a violent way). When the additives leave the tape (in a slow and non-violent way) during burnout process, pores are formed in the micro structure as a result of the leaving. These pores are desirable, especially for the anode and the cathode layer, which is suppose to be porous anyway. Eventually when the burnout process is over, the furnace ramps up the temperature to 1300 °C where it dwells and sinters for 5 hours. Lastly when sintering is finished, the furnace slowly ramps the temperature down to zero and the program is over.

3.3 Micro-structural analysis

A new installed state-of-the-art AFM supplied by Park Systems was used to do micro-structural analysis. A number of samples were analyzed, where it was possible to study the degree of dispersity, particle size, porosity and the tendency of agglomeration during sintering in the samples.

3.4 Electrochemical Evaluation

3.4.1 Substrate Test Setup

Substrate tests are carried out to evaluate and verify the performance of the materials used, to electrochemical characterize and observe thermal and redox stability in the substrates produced. The tests are performed on square samples, where the total area size is between 2 - 4cm^2 and the cathode about 1 cm^2. The sample is placed in a seal-less set-up consisting of two spring loaded flanges with a gas inlet on each side, as can be seen in Figure 3.15. When ready, the whole rig is turned upside down, and lowered into a test furnace, where the rig itself also works as the furnace lid. The test furnace is programmable in the same way as the sintering furnace.

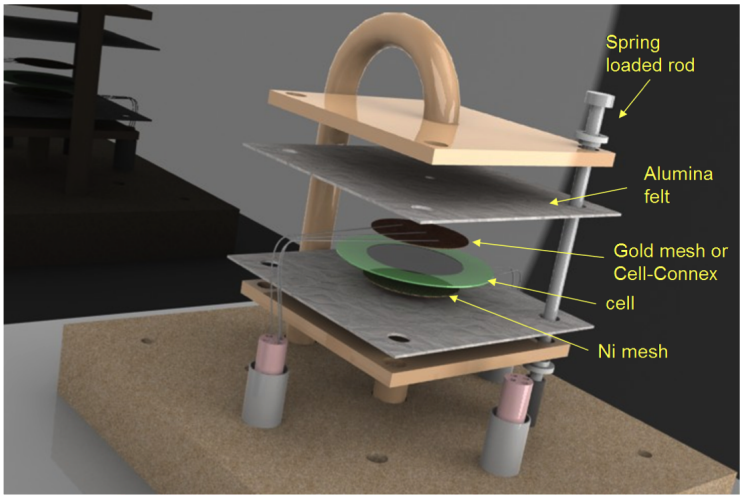

Figure 3.15: SOFC single cell test setup [27].

For a single cell example, current collectors of nickel mesh is pressed against the anode side and a crofer mesh to the cathode side, in this way the current and potential of the fuel cell is measured during the tests. As seen in Figure 3.15 the cell is kept between porous alumina felts to allow gas flow and offer electrical insulation. A thermocouple is placed nearby the active cell area to allow for cell temperature measuring, this is pictured in Figure 3.16 from the actual setup. From a controller desired gas flow rates are set or shut off via flowmeters, which are connected between the gas cylinders and the furnace flanges.

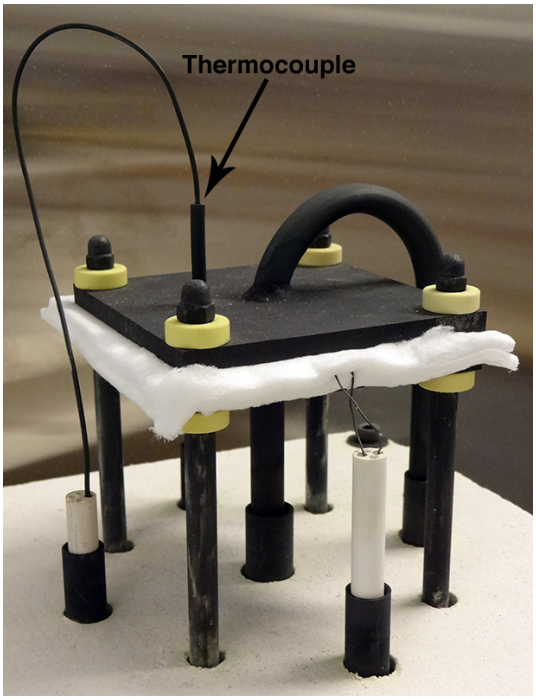

Figure 3.16: Actual single cell test set-up for this project.

For handling hydrogen in general, not only in the laboratory, several safety measures must be taken into account. Below in Table 3.5 some hazard points are listed. When supplying hydrogen to the operating test furnace, it is crucial to consider the present conditions. Take for example, if there is a big share of oxygen in the furnace and the temperature is around or below 585 °C, an extremely dangerous situation can occur at this point if hydrogen is introduced. Firstly, a volatile mixture of oxygen and hydrogen is created, secondly, if the temperature should rise and reach the self ignition limit, an an explosion will possibly happen.

Table 3.5: Characteristics of Hydrogen [39].

Description	**Unit**	**Value**
Self ignition temperature	K (°C)	858 (585)
Min. ignition energy in air	mJ	0.02
Ignition limits in air	vol-%	4 - 75
Flame temperature in air (st.)	K (°C)	2318 (2045)
Detonation limits in air	vol-%	13 - 59
Explosion energy	kg TNT/kg gas (NTP)	2.02

NTP = normal temperature and pressure, T=293.15 K, p=1.013 bar.

st. = stoichiometric mixture i air.

Under controlled conditions, at for example 800 °C, unused fuel burns at the edges of the cell together with the air coming from the cathode [19], as illustrated in Figure 3.17. Since the temperature in this situation is far past the self ignition limit, the hydrogen burns before it gets the chance to accumulate to dangerous levels.

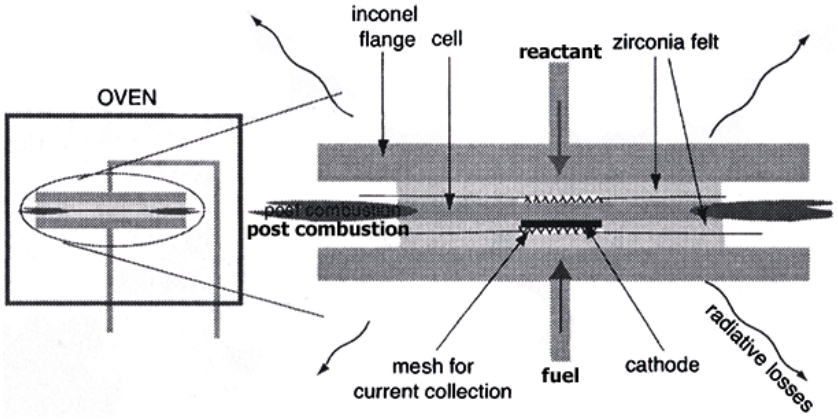

Figure 3.17: Set-up for single cell testing. [19].

3.4.2 I-V Characteristics

The sample is set up in the test furnace, where it is heated to 810 °C and hydrogen-thermal reduced. When the sample has reached a stable condition, with temperature and gas flow as fixed as possible, the testing is ready to begin. The current and voltage is measured with a 4-wire current collector set up, which is coupled to an electronic variable load. With the variable load, the current is controlled. Starting with an open circuit measurement, the current is stepwise increased through a series of values. As soon as the system has stabilized for each new set current value, the corresponding voltage and fuel gas rate are recorded.

3.4.3 Electrochemical Impedance Spectroscopy

For the impedance spectroscopy, a 'Gill 8' made by ACM Instruments, were used for measuring the impedance spectra of the samples. The instrument was connected to the test specimen with only a regular 2 point connection, as it was not possible with a four-wire measurement setup between the equipment and the tested samples. The instrument was provided with a RS-233 serial interface for communicating with a computer, where it is operated via the supplied software from the instrument vendor. The software includes several different test programs and a series of tools for analyzing and presenting results.

Chapter 4

Discussion and Results

In this chapter, the production and evaluative experiment results are presented and discussed.

4.1 In-house Experimentation and Production

4.1.1 Film Applicator

The 3D-printed main parts showed sign of shrinkage after cooling, which is a known case to 3D-printed ABS (acrylonitrile butadiene styrene) plastics. This made the bottom of the guide walls curved, which made the model unstable on the ground. The problem was solved by taping two strips of sandpaper to a straight surface, as displayed in Figure 4.1, and then by putting some pressure on by hand, the bottoms were sanded flat and stable. Because of this, every model made needs calibrating and may not produce the same high precision results.

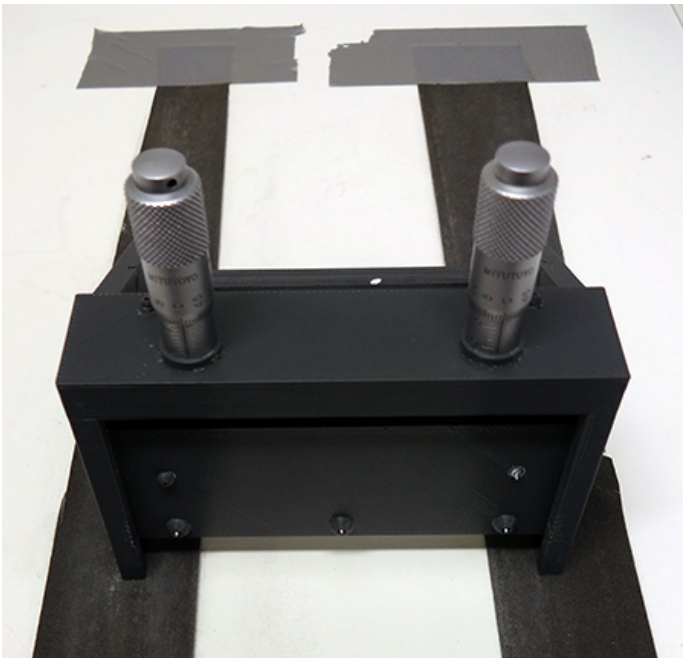

Figure 4.1: Stabilizing and improving model accuracy by sanding the guide walls bottom model flat and even.

The same grinding process was also used to calibrate and align the doctor blade together with the micrometer heads. As a result the micrometer heads now show nearly the same value while the blade is parallel to the glass plate. With some setup time, the tape caster is able to make about 50 µm thin layers. A picture of two complete models is shown in Figure 4.2. The final results turned out very well.

First and foremost, since the tape caster is mostly made of plastic, it is a fragile piece of equipment. On the other hand, if it should break, it is replaceable by printing a new model. Where the expensive parts, the micrometer heads and springs, are just transferred and reinstalled.

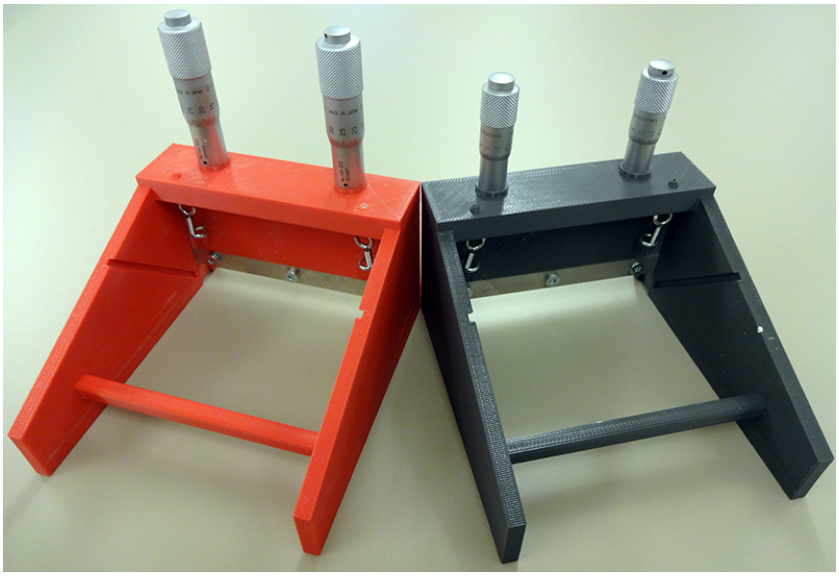

Figure 4.2: Two copies of the model was produced.

4.1.2 Slurry Composing and Film Fabrication

Both YSZ and titania recipes were well optimized and proved good results. Since **YSZ**-electrolyte is meant to be fabricated in a very thin layer, the slurry was made with a rather low viscosity so that it would distribute easily when tape casted. Titania on the other hand had to be tape casted in thicker layers, this in order to have the required strength allowing it to be tested as a standalone substrate.

Titania mixed with $\leq$20% water displayed non-newtonian properties, which abated with an increasing water ratio. The same type of behavior that could be seen when corn flour is mixed with small amounts of water. When using water as the sole solvent, the slurry had poor performance under vacuum. Because the air bubbles bursted too late, which resulted in foam production. Even when adding an amount of defoamer (Propanol), the slurry still did not show satisfying behavior. At this point the decision to flip the ratio of the defoamer and water was made, turning Propanol into the main solvent. An amount of Aceton was also added. Which worked very well, and made the vacuum process extra user friendly.

However when the slurry was tape casted, it showed surface skin formation. Which probably could be a consequence of the significant share of alcohols in the slurry, thereby causing a very high evaporation rate on the surface. Skin formed after just 30 seconds, which made the slurry quite problematic to work with while tape casting. Consequently the water was increased and Propanol and Aceton ratios was decreased until the unwanted behavior disappeared. Secondly the slurry showed a tendency to fragmentation and splitted into several regions while drying, which can be seen in Figure 4.3. It is likely to assume that the amount of alcohols still contributed to

unwanted behavior upon drying, as the fragmentation disappeared as the alcohols were reduced even more.

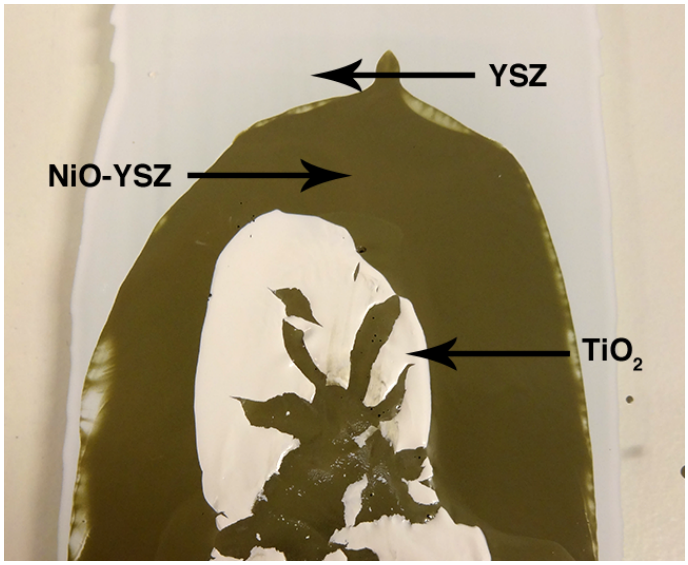

Figure 4.3: Titania slurry tried tape casted on top of NiO-YSZ anode layer. Same fragmentation behavior was also experienced when depositing titania alone as a single layer.

After optimizing the titania recipe, it was discovered that the slurry still behaved differently than a newtonian liquid, such as water. As the final recipe is, the slurry behaves in the same way as ketchup and runny whipped cream do. A property known as shear thinning, a fluid with this property is also known as a pseudoplastic. The viscosity of a pseudoplastic decreases with an increasing rate of shear stress applied parallel to the materials cross section. For example when tilting the slurry container, the slurry will flow faster as the decomposed gravitational force parallel to the inclined slurry increases, see Figure 2.1 for illustration.

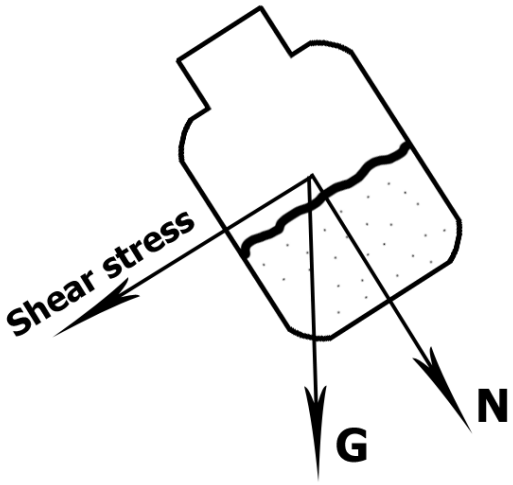

Figure 4.4: One of the decomposed gravitational force components acting as shear stress on titania in conjunction with its shear thinning property.

The consequence of this behavior is a more user friendly slurry. Even though it may seem "thin", it is only so on tilted surfaces and during inflicted movement. However, when deposited on the film carrier under steady conditions, it acts like whipped cream on a cake, not as thick but it stays put. As the doctor blade is dragged across applying shear stress, the slurry flows and distributes smoothly. For this reason it is easily tape casted in thicker layers in the range of 1 - 2 mm.

As a consequence to time constraints, it was not possible to reach a fully optimized slurry recipe for the **NiO-YSZ** anode. But the results so far, proves it rather challenging to produce a slurry that is user and process friendly at the same time. As for the ball-milling and vacuumizing process, it is desirable to have a less viscous liquid to allow the grinding medium to work properly, and bubbles to burst easily. On the contrary, it is desirable to have a more viscous cermet slurry when tape casting, allowing for thicker films to be fabricated.

If titania is to be mixed together with NiO-YSZ, the rheology of it will probably need to be rediscover. And it will also require a different mixture of additives to reach an optimized recipe.

4.1.3 Sintering and Visible Results

After finding proper and inert support plates, alumina type, it was possible to further optimize the sintering process. Using powder beds both underneath and above, together with a slight weight, proved necessary to yield flat substrates without becoming fixed to the support plate.

As stated in the slurry section, the titania recipe was well optimized and provided good samples.

In Figure 4.5 a titania substrate is shown before and after sintering, where the end result was a testable sample with a shrinkage of about 22%.

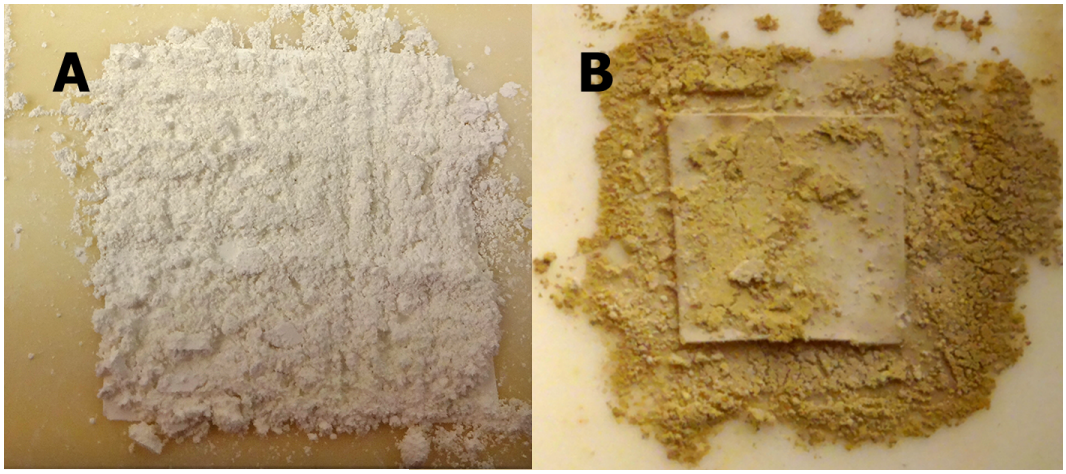

Figure 4.5: (A) TiO_2 tape prepared for sintering with powder beds on top and beneath, in addition a light weight is finally put on top to keep it from curling. (B) Successfully sintered at 1300°C, and in one piece. About 22% shrinkage.

It would be beneficial to optimize the sintering preparation of the tapes even more, so that the substrates turns out smoother, as a means to increase surface contact between the sample and current collectors. This will lead to better and truer measurements of the samples tested.

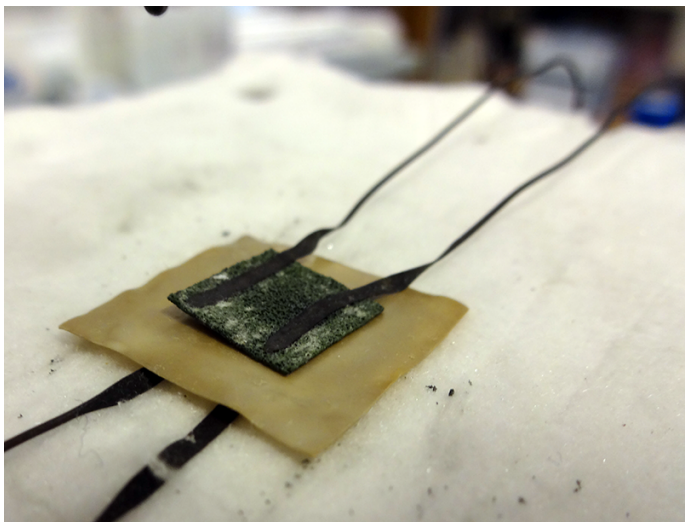

Figure 4.6: Sample B1. Substrate from Figure 4.5 set up for testing in the test furnace. Dimensions: 15.5 x 15.5 x 0.23 mm.

Fabrication of the co-cast cermet and electrolyte had problems with resulting delamination after sintering. Which is thought to occur due to the slurry tape casting delay, before applying the next layer. If the first layer dries to much, the layers will not bond sufficiently and lead to poor adhesion.

The cermet slurry should be applied while the electrolyte layer is still wet, which will be within a period of one minute. It is reasonable to assume that this will increase the adhesion and decrease the resulting delamination.

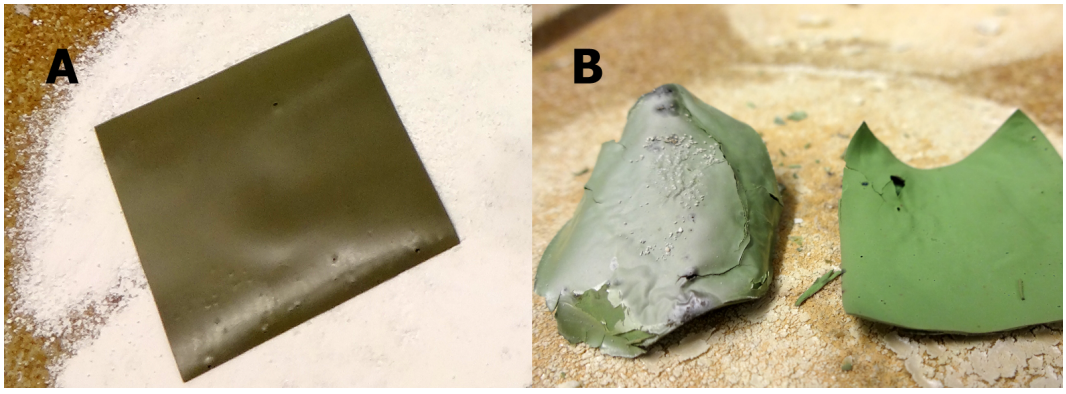

Figure 4.7: (A) Co-casted NiO-YSZ and YSZ prepared for sintering, just with powder bed beneath. (B) Unsuccessfully sintered at 1400°C. Curling and delamination.

A picture of the final sintered co-cast anode and electrolyte substrate is shown in Figure 4.8. The sample shrunk and broke into numerous pieces, except for the big center piece. Could the powder beds induce reactions in the sample, which could lead to fracturing? These speculations were disproved as powder beds of titania gave the same results. The assumption is therefore that it is the slurry recipe which is the erring factor in this case, and needs extensive experimentation.

Figure 4.8: Final co-cast anode and electrolyte substrate, sintered at 1300°C. Unsuccessful result.

4.2 Micro-structural Validation

4.2.1 Titania

Micro-structural analysis has been used to study and learn how different processes affects the titania structure, when being a tape, to sintered substrate and after testing. Figure 4.9A shows a 10 x 10 µm scan of the structure of a standalone unsintered titania tape. Particles are well spread and show good dispersity, where the biggest particles measure less than 1 µm. In other words, the slurry is finely ground and the additives which contribute with dispersing properties are working well. In Figure 4.9B the same sample is sintered at 1300°C. Sintering leads to agglomeration, and in this case medium sized grains at about 2 - 3 µm are formed with an amount of porosity. In Figure 4.9C, the same tape is sintered at 1350°C. And only by an 50°C increase in temperature, more than doubles the grain growth, leading to grains in the size of 5 - 8. Both Figure B and C displays a degree of porosity, which is desired in an anode cermet.

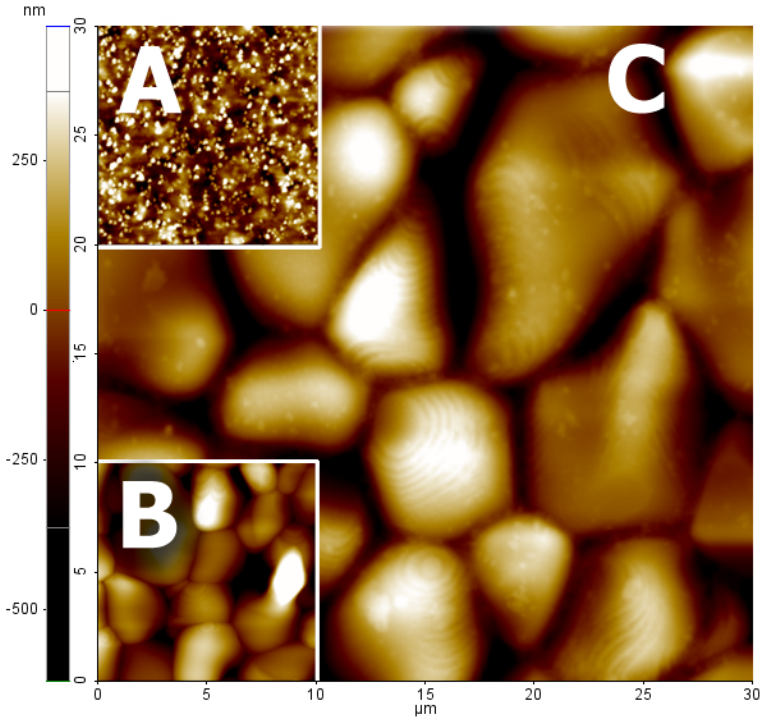

Figure 4.9: Identical magnification for all scans. A: Unsintered, B: Sample B1, sintered at 1300°C, C: Sample C1, sintered at 1350°C.

Smaller grains lead to an increased specific surface area, and titania is supposed to act as an electronic conductor in the anode cermet. A higher specific surface area between titania grains in the porous anode structure would lead to better electronic contact. Which makes it reasonable to suggest that it will be beneficial to keep the titania grain size below a certain limit, to attain good

electronic conductivity.

After sample B1 had been hydrogen-thermally reduced, electrochemical tested and reoxized, it was scanned once more. Figure 4.10B show two different locations from the untested sample, while 4.10A is after testing. The analyzes do not show any significant difference. To possibly spot Magnéli sites on the sample structure after testing, it would be necessary to cool down the sample in a sustained hydrogen reduced environment. This would slow down the reoxidation process, allowing for analysis to be done before the sample is fully reoxidized.

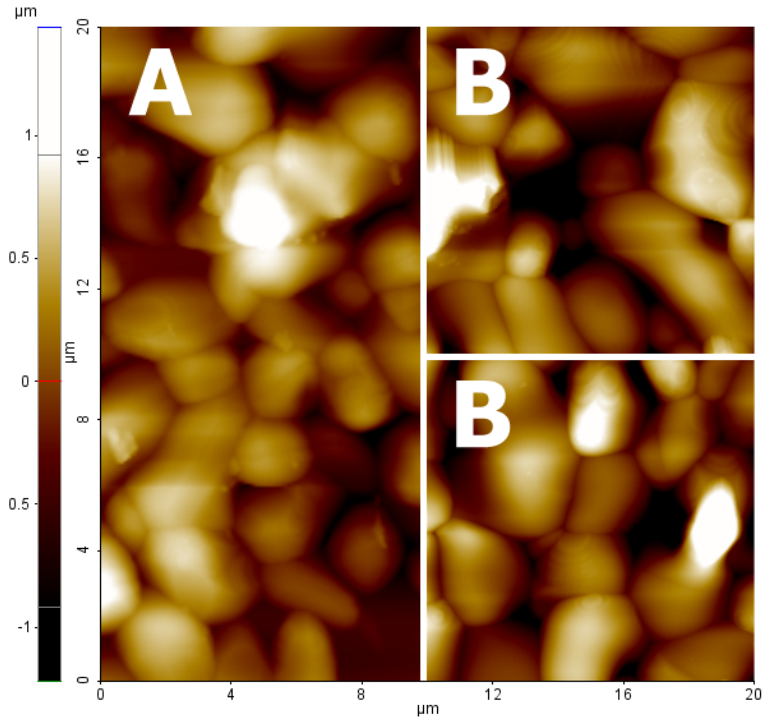

Figure 4.10: Sample B1. Identical magnification for all scans. A: After one hydrogen-thermal reduction cycle up to 850°C, B: Before before hydrogen-thermal reduction, two different locations.

In Figure 4.11 a different location on the tested sample B1 is shown. Neither this scan show any significant difference after testing. Why are there not any differences? It could be, that higher temperature and longer exposure to high temperatures could lead to e.g. sintering and agglomeration. Which in the long run would cause bigger grains and reduced conductivity. This are just assumptions, and can only be confirmed by more and prolonged testing.

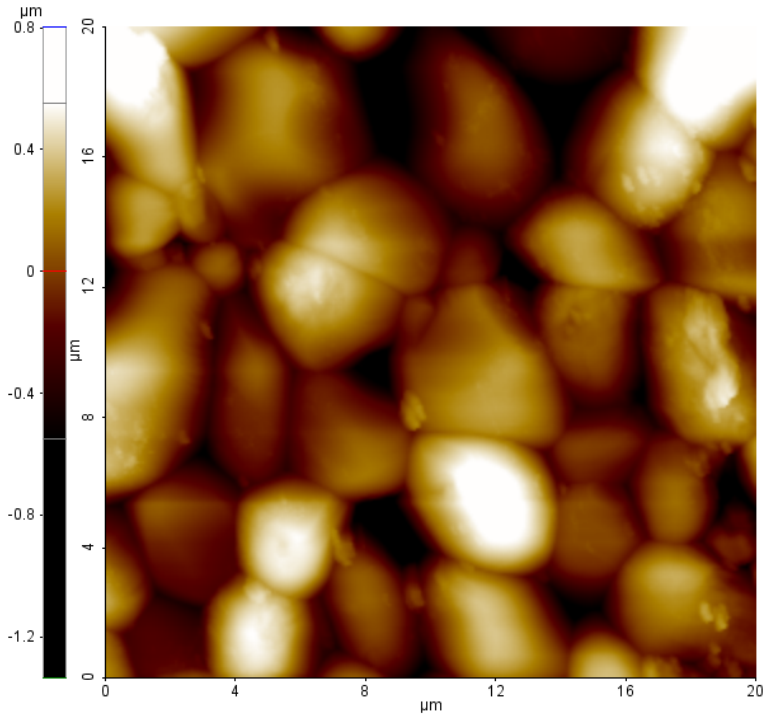

Figure 4.11: Sample B1 after testing, showing a different scan location than Figure 4.10A.

4.2.2 NiO-YSZ

Micro-structural analysis of the final NiO-YSZ anode substrate, presented in Figure 4.12, shows extremely high porosity and may be the reason for it being very brittle and fragile. Which could contribute to having the sample fracture more easily under high thermal stresses, during shrinking.

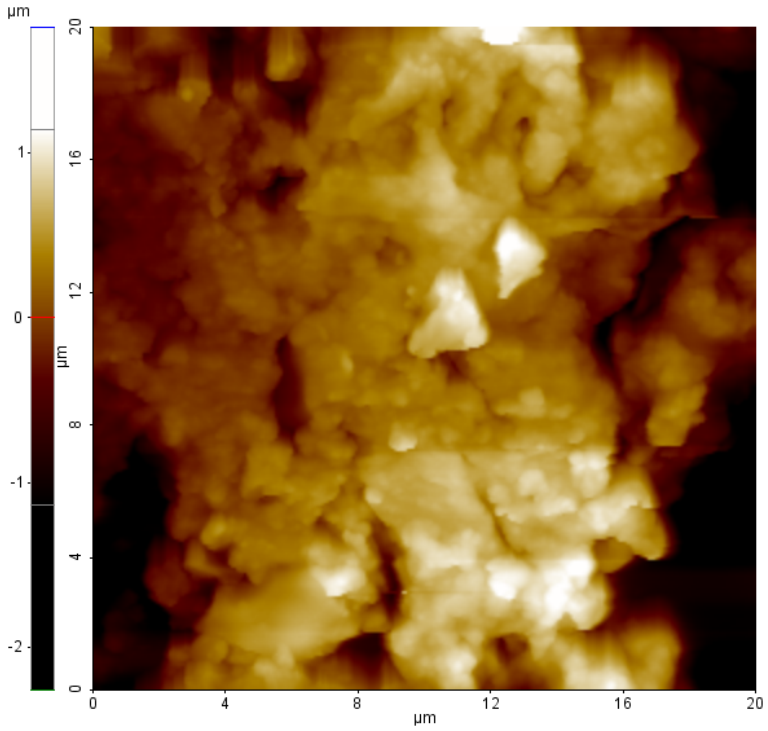

Figure 4.12: Micro-structural analysis on the NiO-YSZ side of the final co-cast NiO-YSZ and electrolyte substrate.

4.3 Electrochemical Characterization

4.3.1 Titania

Three standalone titania samples were tested after one another in the test furnace, where the samples proved coinciding results. For each sample, the furnace was heated to 810 °C in a ambient air environment, and the resistance of the sample was measured with a multimeter. Still measuring, the sample was introduced to a 50/50 hydrogen and nitrogen reduced environment, which made the resistance rapidly decrease. The nitrogen is present in the start for safety measures, to avoid volatile H_2-O_2 mixtures to occur until the oxygen share is significantly reduced. After two minutes the nitrogen was shut off, resulting in only pure hydrogen being supplied. From this point on, the reduction rate started to decrease, which assumably are a result of transition from surface to solid state diffusion inside the sample. Starting at 45kΩ, the multimeter showed 30Ω after 5 minutes. The reaction process is illustrated over time in Figure 4.13.

After stabilizing for a whole night, new measurements were made with a four wire setup for better accuracy. A power supply was connected and 0.5 A imposed on to the sample. The voltage response was measured with a multimeter, and by using Ohm's law the calculated resistance

showed 1Ω. Still, some resistance can be accounted for coming from the measurement wires, resulting in a sample resistance lower than 1Ω. Since the University do not have a x-ray diffractometer (XRD), it cannot be verified if the samples possessed sites of Magnéli phases due to the resulting low resistance.

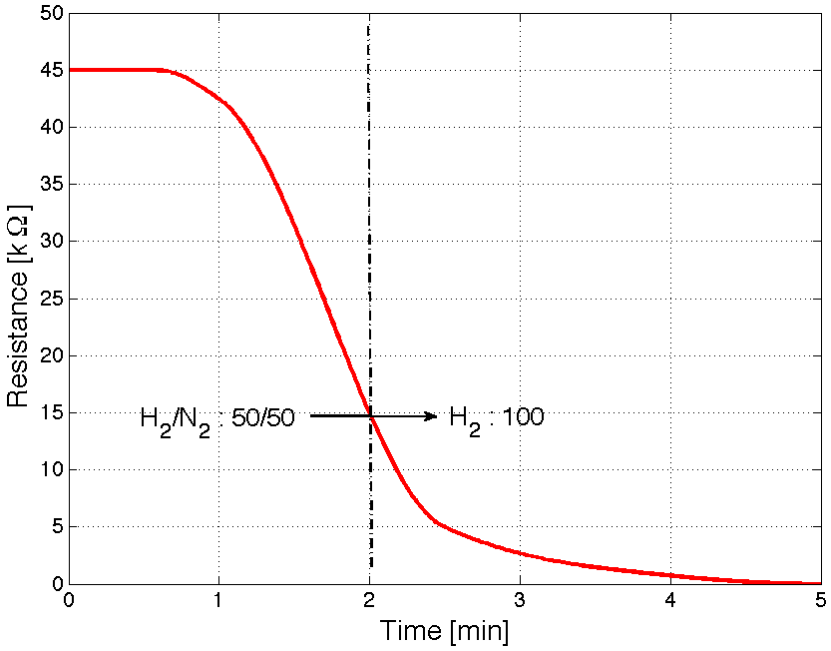

Figure 4.13: Hydrogen-thermal reduction reaction of titania over a timespan of 5 minutes, with end value R= 30Ω.

AC impedance spectroscopy was used to collect impedance data for modeling the Arrhenius plot of a reduced titania sample, where the real impedance part was collected at 0.1Hz (close to DC voltage). The measurement showed small amounts of noise, that could be coming from the whole setup which could be canceled out by earthing the equipment. On the other hand, the noise is not a serious problem, while the measurements illustrate adequate characteristics. The test sample was measured with 1x1 cm^2 current collectors, which gives a 1 cm^2 active test area of the sample. The impedance sweep was made with an 100 mV AC signal starting at 100 kHz and ending at 0.1 Hz. In this study there were some limitations to the measurement. Since the test furnace did not have an oxygen sensor, it was not possible to measure the oxygen partial pressure during testing. Thus there was no reference electrode used, and it was just connected to the same point as the auxiliary electrode.

Before hydrogen reducing the sample, the spectra of stoichiometric TiO_2 was collected. Figure 4.14 show the impedance spectra of a titania sample at 800°C. The coarsely fitted curve is quickly drawn by hand just to show a possible smoother spectra. The fitted curve shows at least three resistor-capacitance networks, resulting through high to low frequencies.

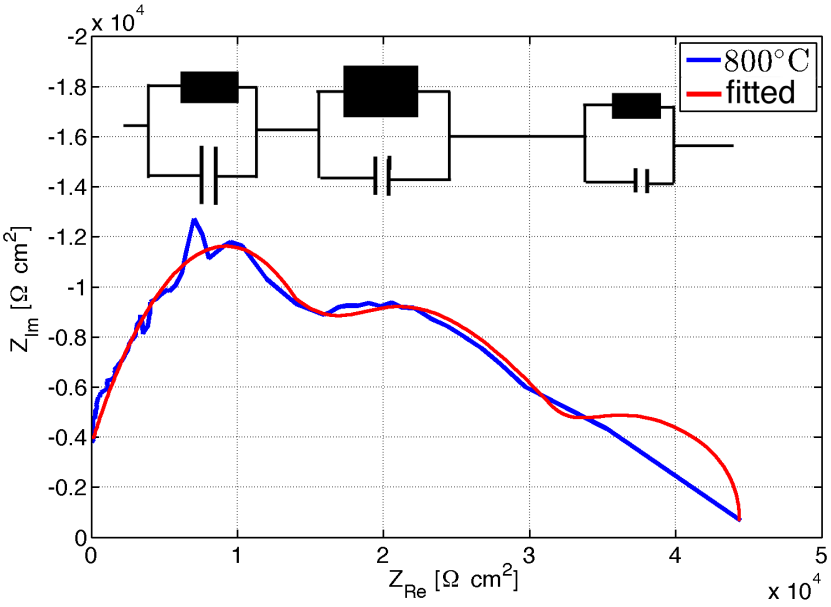

Figure 4.14: Impedance spectra plot of stoichiometric TiO_2 at 800°C (100 kHz to 0.01 Hz).

Studying the impedance spectra in Figure 4.15, the impedance evolves as the temperature increases, from right to left. Focusing on the transition between 800 and 825 °C, we can spot a significant change. The imaginary part of the impedance starts to evolve drastically as temperature increases, while the change in DC resistance decreases. The applied EIS instrument had an upper limit of 100 kHz. Because of this, it was not possible to acquire the more complete impedance characteristics. This can especially be seen at the two highest temperatures, which shows two partial semicircles that starts in "mid-air".

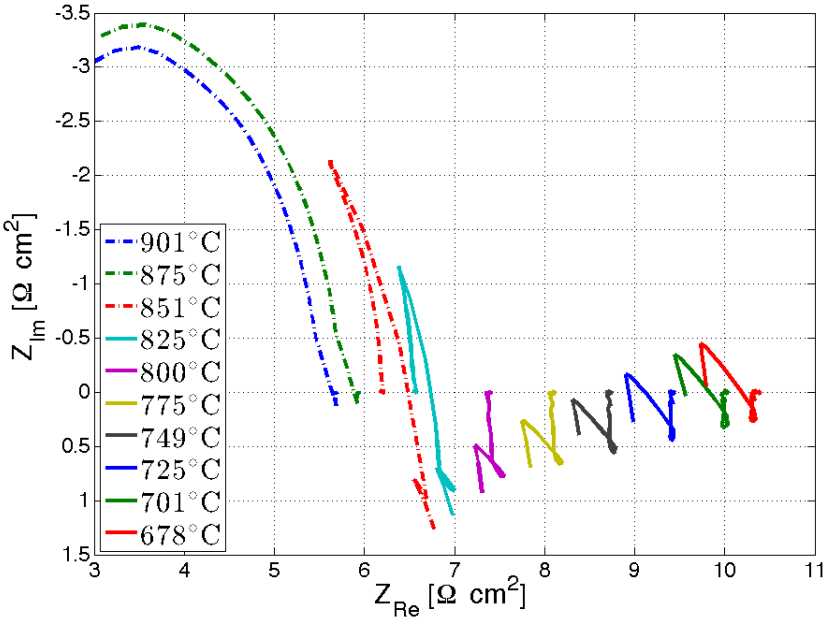

Figure 4.15: Impedance spectra plots for nonstoichiometric TiO_2 at different temperatures (100 kHz to 0.1 Hz, 678 to 901 °C).

Even though not complete, the partial semi circles do show a tendency to titania having a resistor-capacitance (RC) network at high frequencies, especially in the higher temperature region. As Regonini et al. [33] explains in their paper, the XRD verified reduced titania is a mixture of Magnéli phases and stoichiometric TiO_2 areas. Where the resistor in the RC equivalent is represented by the Magnéli generated sites, whereas the capacitive sites correspond to the stoichiometric and more resistive TiO_2 areas. Focusing on this study's impedance spectra (IS) for 875 and 901°C in Figure 4.15, it shows that the conductivity rises and the network capacitance falls at higher frequencies. Since there is no opportunity to verify the quantity of the different phases of TiO_2 in the sample, the impedance spectra only gives room for speculations that can be supported by similarities in the findings of Regonini et al.

However, the Magnéli phases generated in the study of Regonini et al. was produced through carbothermal reduction before testing, and subsequently electroded with Au to minimize reoxidation. And for additional measures to minimize reoxidation during testing, temperatures higher than 375°C were not tested. In this study, the samples were subjected to hydrogen-thermal reduction in situ of/to the testing. Since the test sample is kept in a sustained reduced environment, it allows for testing at higher temperatures without the present chance of reoxidation.

As Liborio and Harrison [23] puts it, "As the oxygen chemical potential is decreased, the structure of the material changes from one Magnéli phase to the next in order to accommodate the larger number of defects." Without knowing for certain, there could be several different Magnéli phases in the reduced samples in this study. It is reasonable to assume, that there is a greater chance

of having phases containing combinations of Ti^{4+} and Ti^{3+}, than having combinations including Ti^{2+}. A Ti - O phase diagram is illustrated in Figure 4.16. The diagram shows how TiO_2 changes from different Magnéli phases due to the decreasing oxygen as a result of temperature and reducing environment.

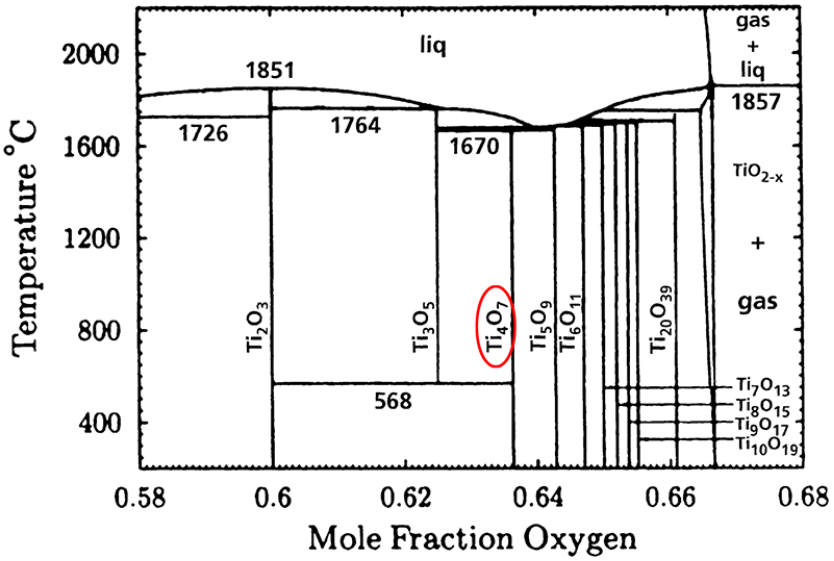

Figure 4.16: The high-temperature region of the Ti - O phase diagram in the composition range between Ti_2O_3 and TiO_2 according to Waldner and Eriksson [38],[2].

An example of the possible combinations of the Magnéli phase Ti_4O_7 is shown below. Since the chance for Ti^{2+} is much lesser than the chances for Ti^{3+} to occur, it is more likely that sites of combination (4.3) are present, instead of (4.4).

$$Ti_nO_{2n-1} = Ti_4O_7 \tag{4.1}$$

$$O_7 = 7O^{2-} \qquad = -14 \tag{4.2}$$

$$Ti_4 = 2Ti^{4+} + 2Ti^{3+} \qquad = +14 \tag{4.3}$$

$$Ti_4 = 3Ti^{4+} + Ti^{2+} \qquad = +14 \tag{4.4}$$

Comparing Figures 4.17 and 4.18. It seems that the lower temperatures of Figure 4.17 shows some similarity to Figure 4.18a in the same regions. While the higher temperatures in Figure 4.17, draws more towards a behavior similar to the upper region of Figure 4.18b.

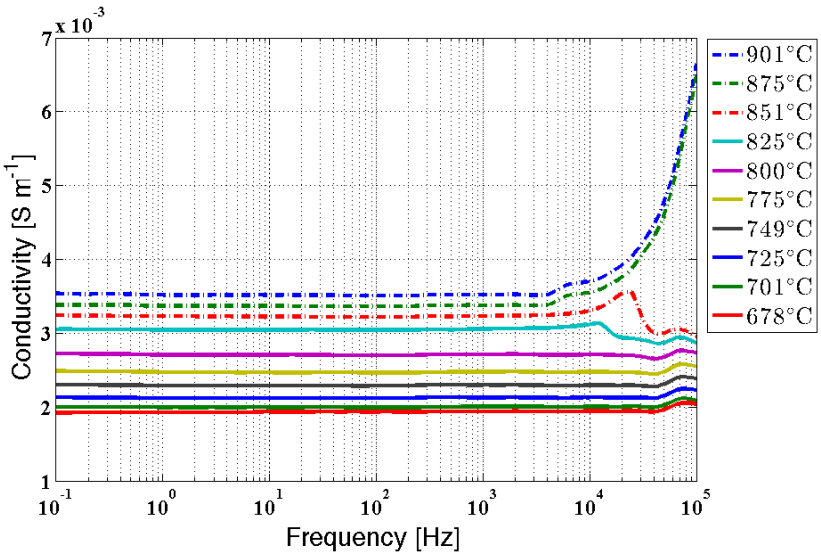

Figure 4.17: Conductivity of hydrogen-thermal reduced TiO_2 substrate over a range of frequency, 0.1 Hz to 100 kHz, and temperatures 678 to 901 °C.

Apart from behavior, the degree of conductivity measured in this study coincide somewhat with the values measured for TiO_2 in Figure 4.18a. Even though they do not show the exact same degree of conductivity at the same temperatures, it can be a result of several factors. As mentioned earlier, the samples in this study are not perfectly flat, which can lead to an decreased contact surface conductivity towards the current collectors.

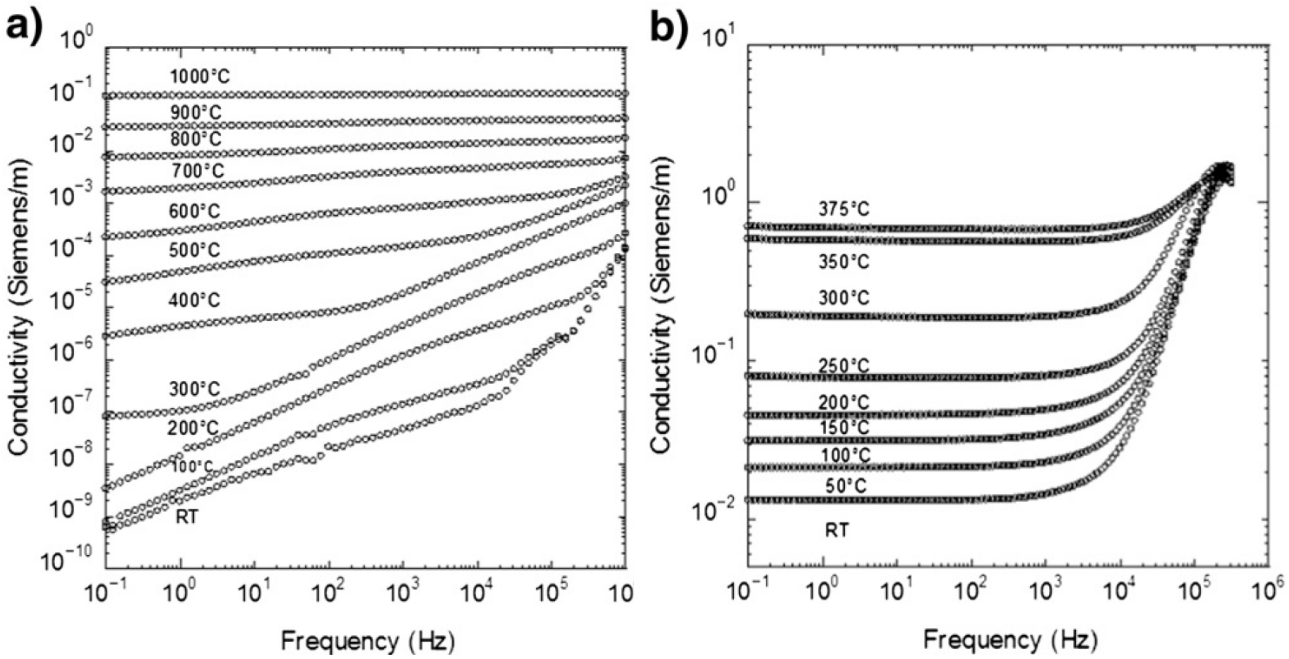

Figure 4.18: Conductivity of TiO_2 over a range of frequency, (a) 0.1 Hz to 1 MHz, and temperatures, RT to 1000°C, (b) Ti_nO_{2n-1}, 0.1 Hz to 100 kHz, RT to 375°C [32].

With conductivity similar to the values of TiO_2 and matching behavior towards that of Ti_nO_{2n-1} in Figure 4.18. Based on observations and referred work, it gives reason to believe that the total conductivity in the studied samples is a blend. When reduced, they possess a composition of different phase sites in the range between TiO_2 and Ti_2O_3, as seen in the phase diagram of Figure 4.16. It is safe to exclude that this is not a case of pure Magnéli phase, because the Arrhenius plot shown in Figure 4.20 would then have had a positive slope. Instead, the Arrhenius plot in Figure 4.20 clearly show the behavior of a n-type conductor.

After finishing testing and shutting of the hydrogen supply, the IS of a reoxidized sample was also collected. This gave the opportunity to see the difference between before and after hydrogen reduction. It shows that the titania sample recovers some of its semicircle characteristics after being reoxidized, in addition to having both decreased real and imaginary impedances. Still, it is reasonable to believe that the impedance values will increase over time as the sample is further reoxidized.

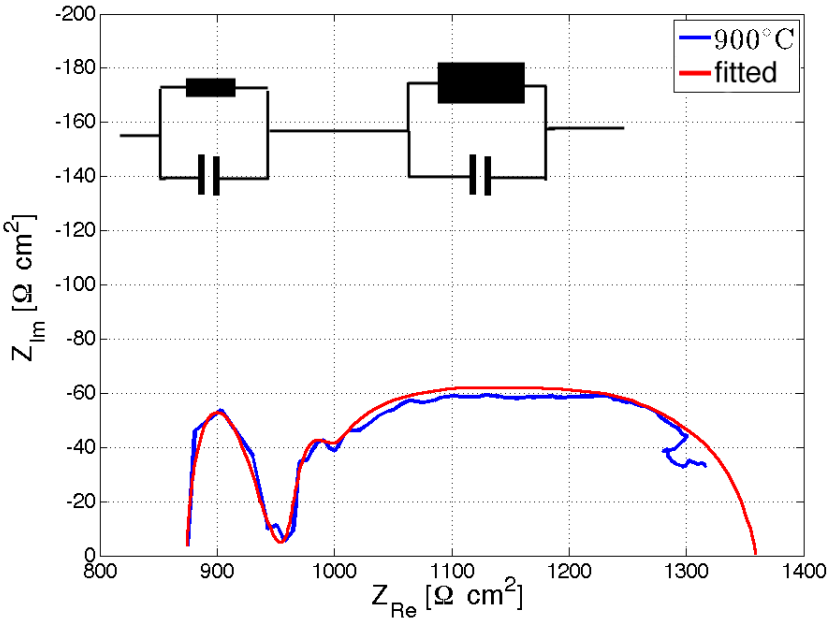

Figure 4.19: Impedance spectra plot of TiO_2, reoxidized at 900°C after being being hydrogen reduced (100 kHz to 0.1 Hz).

The Arrhenius plot in Figure 4.20 do also show a change in the same area as aforementioned for the IS in Figure 4.15. This gives reason to assume that there are two reaction processes, and therefore two different activation energies. Based on this observation, linear regression was performed on each of these regions.

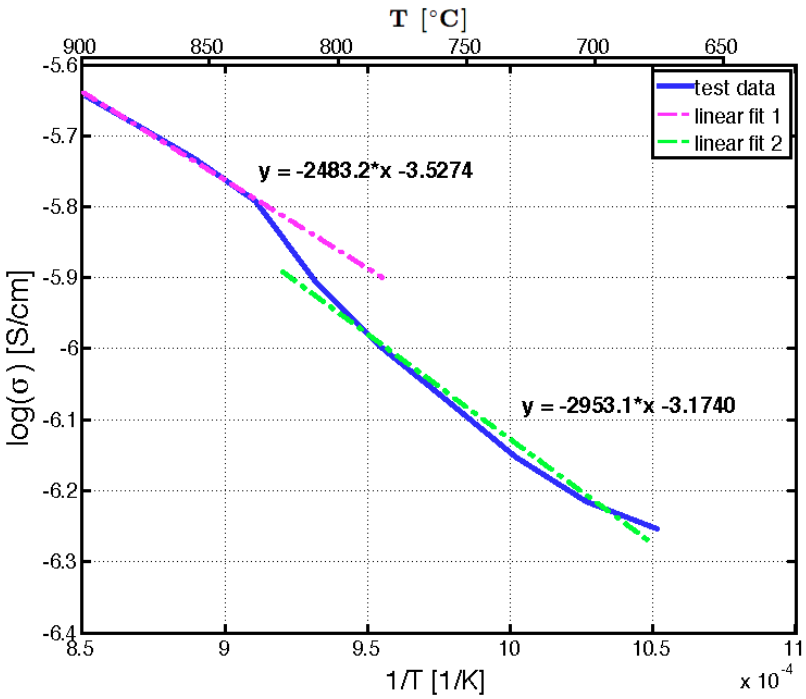

Figure 4.20: Arrhenius plot of reduced titania.

By using linear regression in Matlab, the equation values were found and plotted together with the test data, which is illustrated in Figure 4.20. Further, the activation energies (2.18) and pre-exponential factors (2.19) was calculated from the equation. Results are listed in Table 4.1.

Table 4.1: Activation energy and pre-exponential factor

Linear fitting	**Activation energy** (E_A) $\begin{pmatrix} kJ\ mol^{-1} \\ eV \end{pmatrix}$	**Pre-exp. factor** (σ_0) ($S\ m^{-1}$)
Linear fit 1	20.65 ± 0.03 0.21	2.94 ± 0.01
Linear fit 2	24.55 ± 0.23 0.26	4.18 ± 0.04

The activation energies found in this study do not coincide with any of the other studies. They appear lower than the corresponding work of Regonini et al. and Liborio and Harrison, 0.77 eV and 0.25 eV, respectively. It should be said, that the other studies have only looked at pure Magnéli phase cases and the activation energies are based on these. While results from this study, most probably stems from the contribution of several different Magnéli phases, which could result in lower activation energies. It could be that this is a plausible explanation, and the reason to why it is difficult to compare the results.

Because of limited study done on this particular field of titania, it has been difficult to find relevant literature to refer to and compare with. The work of regonini et al. was the most corresponding work which was found during the project, through the channels that were available.

4.4 Thermal and Redox Stability

The only redox and stability evaluation that was done, were after each electrochemical test. Only one cycle, where the sample was hydrogen-thermal reduced at 800°C, sustained in a hydrogen reduced environment and heated to maximum 900°C. Afterwards the hydrogen was shut off, and the test furnace turned off, letting the furnace cool down on its own. Without hydrogen, samples will reoxidize fast at high temperatures, due to the fact that the reaction kinetics are increased by the high temperature. As seen in Figure 4.21, this sample did not survive one cycle through the test routine.

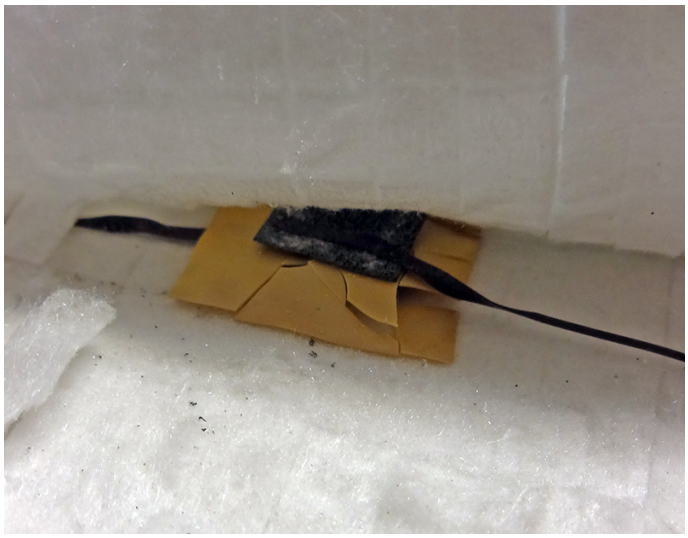

Figure 4.21: Sample C1. TiO_2 substrate sintered at 1400 °C. Hydrogen-thermal reduced at 800°C, and brought up to 900°C. Did not survive one cycle treatment.

In Figure 4.22, the sample did survive the test cycle routine. What could be the reason for these different end results? Sample C1 in Figure 4.21 was heated and tested to a maximum of 900°C, an additionally 50 degrees more than sample B1, which only reached 850°C. It is unlikely to believe that the additional 50°C is the reason why sample C1 cracked. The more likely cause, is the higher sintering temperature leading to bigger grains and a coarser substrate structure. While sample B1 has finer structure. Referring back to the micro-structural analyses. Possessing a higher specific surface area, can possibly lead to a stronger structural frame. Something a mechanical strength test can help to verify, if applied.

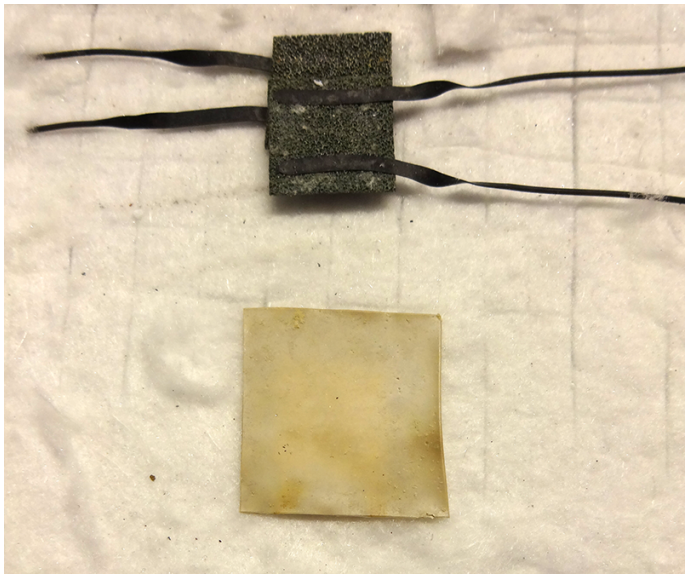

Figure 4.22: Sample B1. TiO_2 substrate sintered at 1300 °C. Hydrogen-thermal reduced at 800°C, and brought up to 850°C. Survived one cycle treatment.

4.5 Summary of Discussion and Results

A big share of the effort laid down into this project has consisted of initial and preliminary work. Due to time constraints, there was no room for extended and repeated experiments to thoroughly verify the findings that has emerged during the project. Because of the setup arrangement it was not possible to go where some of the other studies went, e.g. to lower temperatures under reduced conditions, due to matters of safety. This study moved deeper into the defect chemistry than what was actually planned, compared to what this project originally was set out to do. But the measurements and results that emerged demanded explanation and thus it was necessary to include this field of study.

Besides, to better interpret the results and acquire a greater understanding of Magnéli phases and the chemistry behind it, it will require more sophisticated equipment, something that has not been at disposal. This is the main reason for the amount of speculations and assumptions contained in the discussion, instead of confirmations. Still, the conductivity measurements and the behavior observed from the IS results, do show that titania has desirable traits which can be used in an anode cermet.

Good and assuring results, and insight, has been achieved in other areas of the project. A good tape casting system has been created, and the fabrication and production routines has begun to reach a satisfactory level. Furthermore, some of the slurry recipes has also reached a decent quality in view of the projects limited run. These achievements does indeed involve and touch several of

the main objectives of this project.

Chapter 5

Conclusion

5.1 Introduction

The main intention with this project was to investigate if titania possibly could act as a catalyst in the cermet anode of a SOFC. If so, it could help to reduce the SOFC material costs and make it more adapted for other fuels. This in turn can contribute to commercialization of the SOFC technology. A good anode catalyst need to show high electronic conductivity, offer mechanical strength, chemical inertness and matching TEC towards other materials in the cermet and the electrolyte. To be able to verify any of these properties, it was necessary to produce testable SOFC substrates. First and foremost, creating and setting up a fabrication line was vital to reach any subsequent main goals. Iteration and optimization of processes has been important to attain the required understanding and to improve the reproducibility of substrates. Without proper equipment such as the AFM and EIS the optimization and evaluation processes would not have been as effective and insightful, leading to the results presented.

5.2 Conclusion

The study has shown that it is highly possible to create a low-cost tape casting system. A system able to produce thin films down to a thickness of about 50µm, resulting in a precision well within the requirements of the project. The project has given a good opportunity to work at the material aspect of titania in bulk. Using the tape casting system, it has been possible to produce testable titania substrates from a decent optimized slurry recipe. The results from the micro-structural evaluation show that titania has traits of porosity, and supported by theory it is fair to conclude that it is beneficial to sinter at lower temperature. 1300°C is the better choice for sintering temperature,

which gives smaller grains. Smaller grains are assumed to improve the electronic network and thus increase conductivity, it is also believed to increase structural strength. The EIS results from titania showed that the reduced samples most likely possessed a blend of different Magnéli phases, proven by the increased conductivity and similar behavior to the work done by Regonini et al. [32]. Still, the conductivity did not prove high enough to consider titania as a sole electronic anode material. Because of this, it implies that to reach a satisfactory conductivity level, it is necessary to pair titania together with an additional metallic conductor, such as copper. The project time scale did unfortunately not allow for development and study of a cermet based on titania.

5.3 Further work

Even though the tape casting system works well, it is still possible to do some improvements, as well as there are opportunities to further develop the system. For improvements, an additional and wider glass plate should be acquired. Because from experience, irregularities in the foundation are transferred through the guide walls to the doctor blade, and eventually ends up in the tape. An additional plate would help to reduce these effects, as the film carrier plate and tape caster is placed and operated on the smooth surface of this plate.

The experience coming from the iteration and optimization of the production process has resulted in a written walkthrough for using the tape casting system, which is found in Appendix A: Tape casting guide. This will work as a quick and practical introduction for those who wish to continue the same track or similar work.

From a study in the thermoelectric materials field done by Lu et al. [25], they have looked at the effect from creating composites by adding copper to TiO_{2-x}. It shows that by adding a volume fraction of 12 - 20 % of copper to the nonstoichiometric titania, it is possible to increase the conductivity by a thousandfold. This is certainly something worth following up, and can be useful in further work from this project's study.

Further work

1) Improve and optimize the slurry formulations, to attain better properties and improve better adhesion between component layers.

2) Achieve a better understanding of the sintering process, to control porosity, mechanical strength and conductivity.

3) Look at nonstoichiometric titania and copper composites for SOFC anode catalyst application, and investigate performance and behavior. What could the result be?

4) Create a lab setup for testing materials in a closed compartment, with oxygen partial pressure measurement. This will allow for testing with e.g. ac impedance spectroscopy, in hydrogen reduced conditions at lower temperatures.

Bibliography

[1] W. Beckera, R. Brauna, M. Penevb, and M. Melainab, "Design and technoeconomic performance analysis of a 1 mw solid oxide fuel cell polygeneration system for combined production of heat, hydrogen, and power," *Journal of Power Sources*, vol. 200, pp. 34–44, 2012.

[2] L.-M. Berger, S. S. C.C. Stahra, S. Thiele, M. Woydt, and N. Kelling, "Dry sliding up to 7.5 m/s and 800 °c of thermally sprayed coatings of the tio2–cr2o3 system and (ti,mo)(c,n)–ni(co)," *Wear*, vol. 267, pp. 954–964, 2009.

[3] J. Chen, F. Liang, L. Liu, S. Jiang, B. Chi, J. Pu, and J. Li, "Nano-structured (la, sr)(co, fe)o3 + ysz composite cathodes for intermediate temperature solid oxide fuel cells," *Journal of Power Sources*, vol. 183, no. 2, pp. 586–589, 2008.

[4] W. contributors. (2013, 04) Atomic force microscopy. [Online]. Available: http://en.wikipedia.org/w/index.php?title=Atomic_force_microscopy&oldid=549378370

[5] P. V. Dollen and S. Barnett, "A study of screen printed yttria-stabilized zirconia layers for solid oxide fuel cells," *Journal of the American Ceramic Society*, vol. 88, no. 12, pp. 3361–3368, 2005.

[6] H. Hayashi, T. Saitou, N. Maruyama, H. Inaba, K. Kawamura, and M. Mori, "Thermal expansion coefficient of yttria stabilized zirconia for various yttria contents," *Solid State Ionics*, vol. 176, no. 5-6, pp. 613–619, 2005.

[7] D. Hotza and P. Greil, "Review: aqueous tape casting of ceramic powders," *Materials Science and Engineering*, vol. A202, pp. 206–217, 1995.

[8] I. Inc. (2012, 01) The forms and phases of zirconia engineering ceramics that lead to high strength and toughness. [Online]. Available: http://www.azom.com/article.aspx?ArticleID=5780

[9] G. Instruments. (2005) Electrochemical impedance spectroscopy primer. [Online]. Available: http://andromeda.rutgers.edu/~huixinhe/courses/electroanalchem/Lec%2011%2012%202012/Impedance,%20preparation%20materials.pdf

[10] ——. (2010, 3) Basics of electrochemical impedance spectroscopy. [Online]. Available: http://www.gamry.com/assets/Application-Notes/Basics-of-EIS.pdf

[11] H. Jua, S. Uhmb, J. W. Kima, R.-H. Songc, H. Choid, S.-H. Leed, and J. Lee, "Enhanced anode interface for electrochemical oxidation of solid fuel in direct carbon fuel cells: The role of liquid sn in mixed state," *Journal of Power Sources*, vol. 198, pp. 36–41, 01 2012.

[12] R. J. Kee, H. Zhu, A. M. Sukeshini, and G. S. Jackson, "Solid oxide fuel cells: Operating principles, current challenges, and the role of syngas," *Combustion Science and Technology*, vol. 180, no. 6, pp. 1207–1244, 2008.

[13] H. S. Kim, J. H. Kang, I.-H. Oh, C. H. Jeong, S. J. Boo, J. H. Jo, and H.-S. Kim, "A study of lscf cathode material prepared by pechini process for it-sofcs," in *International Conference on Power and Energy Systems*, vol. 13. IERI, 2012, pp. 396–401.

[14] W.-H. Kim, H.-S. Song, J. Moon, and H.-W. Lee, "Intermediate temperature solid oxide fuel cell using (la,sr)(co,fe)o3-based cathodes," *Solid State Ionics*, vol. 177, pp. 3211–3216, 2006.

[15] H. Kishimotoa, A. Suzukib, T. Shimonosonoa, M. E. Britoa, K. Yamajia, T. Horitaa, F. Munakatab, and H. Yokokawaa, "Agglomeration behavior of nickel particles on ysz and tio2-doped ysz electrolytes," *Journal of Power Sources*, vol. 199, pp. 174–178, 2011.

[16] ——, "Agglomeration behavior of nickel particles on ysz electrolyte," *Solid State Ionics*, vol. 225, pp. 65–68, 2012.

[17] A. L. Lapidus, O. L. Eliseev, and M. V. Kryuchkov, "Bell–boudoir and water gas shift reactions under conditions of the fischer–tropsch synthesis," *Solid Fuel Chemistry*, vol. 45, no. 5, pp. 313–315, 2011.

[18] J. Larminie and A. Dicks, *Fuel Cell Systems Explained*, 2nd ed. John Wiley and Sons Ltd, 2003.

[19] D. Larrain, "Solid oxide fuel cell stack simulation and optimization, including experimental validation and transient behaviour," Ph.D. dissertation, ÉCOLE POLYTECHNIQUE FÉDÉRALE DE LAUSANNE, 2005.

[20] Z. Leia, Q. Zhua, and L. Zhaoa, "Low temperature processing of interlayer-free lscf cathodes for intermediate temperature solid oxide fuel cells," *Journal of Power Sources*, vol. 161, no. 2, pp. 1169–1175, 2006.

[21] P. Leone, M. Santarelli, P. Asinari, M. Calì, and R. Borchiellini, "Experimental investigations of the microscopic features and polarization limiting factors of planar sofcs with lsm and lscf cathodes," *Journal of Power Sources*, pp. 111–122, 2008.

[22] S. Li, Y. Geng, Q. Zhang, and H. Yang, "Aqueous processing of li1.075nb0.625ti0.45o3 green tapes," *Journal of Ceramic Processing Research.*, vol. 12, no. 2, pp. 155–159, 2011.

[23] L. Liborio and N. Harrison, "The thermodynamics of oxygen defective magnéli phases in rutile: a first principles study," Department of Chemistry, Imperial College London, Tech. Rep., 2008.

[24] C. R. Ltd. Titanium dioxide - titania (tio2). [Online]. Available: http://www.azom.com/article.aspx?ArticleID=1179

[25] Y. Lu, K. Sagara, Y. Matsuda, L. Hao, Y. R. Jin, and H. Yoshidac, "Effect of cu powder addition on thermoelectric properties of cu/tio2-x composites," *Ceramics International*, vol. 39, pp. 6689–6694, 2013.

[26] T. Luschtinetz, "Fuel cells and their technical application," Fachhochschule Stralsund," Powerpoint presentation, 2012.

[27] H. P. Middleton, "Solid oxide fuel cell: Lecture 7," University of Agder," Powerpoint presentation, 2013.

[28] M. Mori, T. Yamamoto, H. Itoh, H. Inaba, and H. Tagawa, "Thermal expansion of nickel-zirconia anodes in solid oxide fuel cells during fabrication and operation," *Electrochemical Society Journal*, 1998.

[29] U. of Cambridge. Fuel cells. [Online]. Available: http://www.doitpoms.ac.uk/tlplib/fuel-cells/printall.php

[30] R. P. O'Hayre, S. Cha, W. G. Colella, and F. B. Prinz, *Fuel Cell Fundamentals*, 2nd ed. Hoboken, New Jersey: John Wiley and Sons Ltd, Inc., 2009.

[31] S. C. Page, A. H. Anbuky, S. P. Krumdieck, and J. Brouwer, "Test method and equivalent circuit modeling of a pem fuel cell in a passive state," *IEEE TRANSACTIONS ON ENERGY CONVERSION*, vol. 22, no. 3, pp. 764–773, 2007.

[32] D. Regonini, V. Adamaki, C. Bowen, S. Pennock, J. Taylor, and A. Dent, "Ac electrical properties of tio2 and magneli phases, tino2n-1," *Solid State Ionics*, vol. 229, pp. 38–44, 2012.

[33] D. Regonini, A. Dent, C. Bowen, S. Pennock, and J. Taylor, "Impedance spectroscopy analysis of tino2n-1 magneli phases," *Materials Letters*, vol. 65, pp. 3590–3592, 2011.

[34] D. Skarmoutsos, P. Nikolopoulos, and A. Tsoga, "Titania doped ysz for sofc anode nicermet," *Ionics*, vol. 5, pp. 455–459, 1999.

[35] D. Skarmoutsosa, A. Tsogab, A. Naoumidisb, and P. Nikolopoulosa, "5 mol-doped ni-ysz anode cermets for solid oxide fuel cells," *Solid State Ionics*, vol. 135, pp. 439–444, 2000.

[36] A. S. Thorel, *Ceramic Materials, Tape Casting Ceramics for high temperature Fuel Cell applications*, W. Wunderlich, Ed. Sciyo, 2010.

[37] P. Tiwari and S. Basu, "Ni infiltrated ysz anode stabilization by inducing strong metal support interaction between nickel and titania in solid oxide fuel cell under accelerated testing," *International Journal of Hydrogen Energy*, vol. XXX, pp. 1–6, 2012.

[38] P. Waldner and G. Eriksson, "Thermodynamic modelling of the system titanium-oxygen," *Calphad*, vol. 23, no. 2, pp. 189–218, 1999.

[39] C.-J. Winter and J. Nitsch, Eds., *Hydrogen as an Energy Carrier*. Springer, 1988.

[40] J. Zhang, Ed., *PEM Fuel Cell Electrocatalysts and Catalyst Layers*. Springer-Verlag London Limited, 2008.

Appendix A

Tape casting guide

This is a quick guide for how to tape cast with the self-made equipment that has been used in this project. The step-by-step explanation gives a kick-start for anyone who is in need for tape casting substrates, but without many of the errors I made till I had found a good routine.

A.1 Slurry Preparation

If you have made a slurry yourself or have bought a ready made one, it is very important that you make sure that the slurry contains as little foam and bubbles as possible. Because if your casted tape is full of air bubbles, it will introduce weaknesses and deformation to your tape when it is dried. To get the air out of the slurry it is practical to use a vacuum chamber, which is to be found in the lab. It is also possible to make a low-cost one yourself, where you find enough tutorials on www.youtube.com. The small chamber found in the lab is pictured in Figure A.1.

Figure A.1: Vacuum chamber driven by a small water pump connected to and driven by a regular water tap.

All depending on the properties of the slurry, it can react slow or fast to the vacuum. The bubbles can burst pretty early, or they can grow big and apparently never break. If the bubbles don't break at any point, the slurry will start to seep over and out of the container you are using. You have to keep an eye on this, because the growth can occur very fast when it suddenly starts.

If the bubbles does not seem to break, there is a quick solution to this. Add a quantity of alcohol with a high evaporation rate, e.g. Aceton. This will in most cases, depending on the materials in the slurry, work as a defoamer, which means that the bubbles will burst before they grow big. And by the time most of the air has left the slurry, the added alcohol will have evaporated.

What you can do, is to have a weight nearby, and weigh the container when you add the alcohol and leave the weight on. Afterwards when you have vacuumed the slurry, you weigh it once more, and you are able to see how much alcohol that has evaporated during the vacuuming.

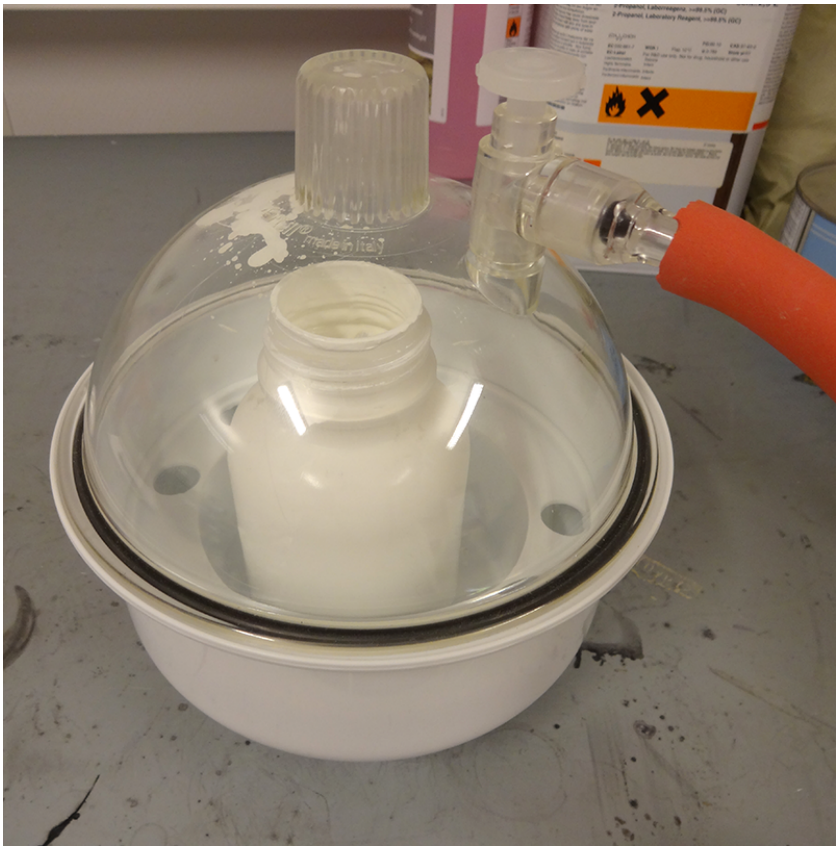

Figure A.2: Complete vacuum chamber, remember to start without the screw. And when attached, at once locate where the "open" position of the screw is.

To use the vacuum chamber, turn the tap water running, put the lid on to the container and attach the tube to the lid connection, without the screw. The screw has an open and close function, so that you can regulate the vacuum to a certain degree. When you attach the screw, locate where "open" is. When you do, you will hear a continuous "hiss" sound.

Observe the slurry, it may take some time until something happens and the slurry can grow a bit before rapid bursts start to occur. Therefore you may have to adjust the screw a bit to counter over-foaming. When bubbles starts to burst rapidly you can close the screw completely. When rapid bursts begins to decrease it is smart to shake the chamber a bit, because there may be bubbles between the milling balls (if there are any) which will then rise to the surface. At the end when there are very few bursts, the most crucial amount of air has left the slurry. But, if you're not in a hurry you can just leave it for some extra time.

A.2 Tape casting setup

Preparing for casting some tapes you will be needing some equipment. If you have different slurries to use, you'll need the same number of pipets, we don't want to mix them. Are you planning on co-casting, that is, casting one layer on top of the other one, e.g. first electrolyte and then anode. Then the best setup will be to have two tape casters, or else you need to be quick to wash the one you have, after the first layer. At last you need a film carrier. As the tape casters are designed to be used with a specific carrier thickness, there is a hardened glass plate tailored to work with the applicators. Be sure to check the orientation of the glass plate, the unscratched side facing up.

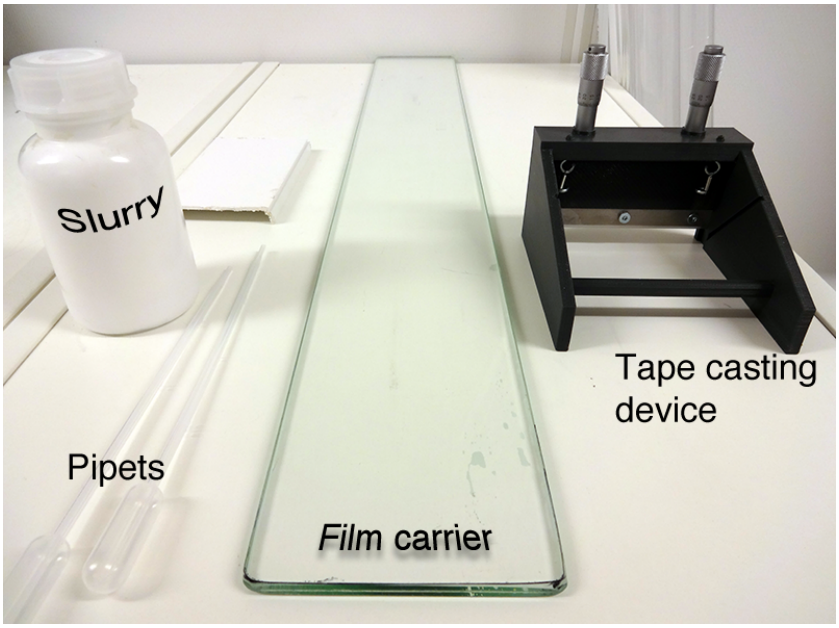

Figure A.3: Equipment needed. Slurry, some pipets, the tape casting device and tailored glass plate (film carrier).

By putting the tape caster above the glass plate, the doctor blade is adjusted close to the glass plate.

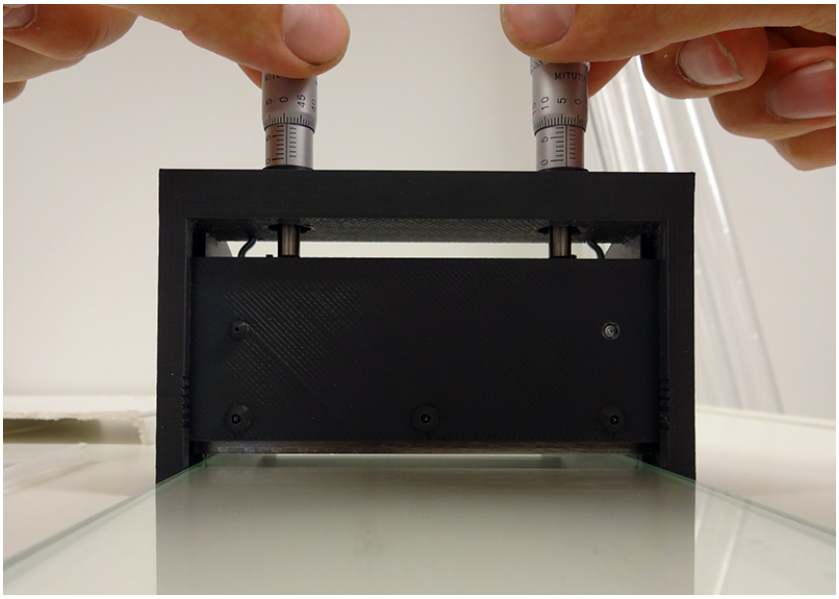

Figure A.4: Adjusting the gap between the glass plate and doctor blade.

As Figure A.5 shows, zero gap for the grey applicator should be around the pictured values. These values can change as the micrometer heads are not permanently fastened to the applicator. Take it as a guide value.

Figure A.5: The micrometer values of the dark grey tape casting device at zero gap.

The other way is to look at the doctor blade as it makes contact to the glass plate, there should virtually travel no light between the glass plate and the blade at zero gap. As an example have a look at Figure A.6. A second alternative is to use feeler gauges, and close the gap until the feeler gauge sticks between the blade and the glass plate. It is practical to have two of them, one for each side.

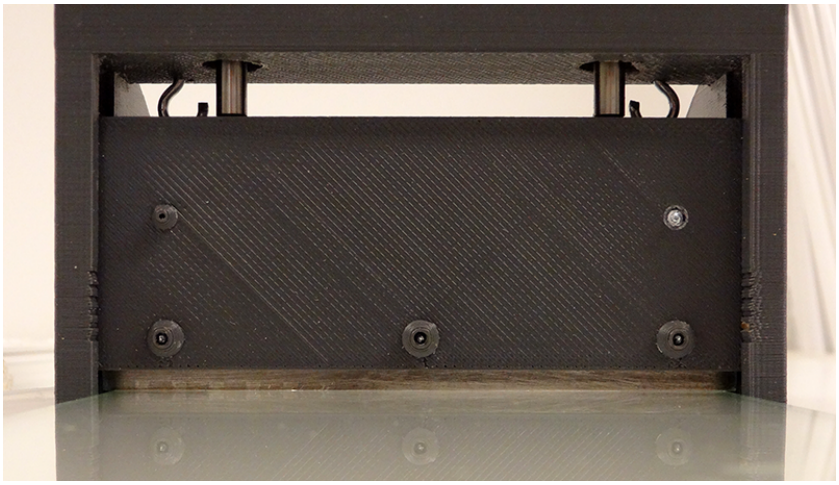

Figure A.6: Zero gap, allowing virtually no light to cross from the bright background to front.

From the "zero gap" position you set the desired thickness by turning back the micrometer heads, retracting half a millimeter by each revolution. When the thickness is set, it is time for depositing slurry on the plate.

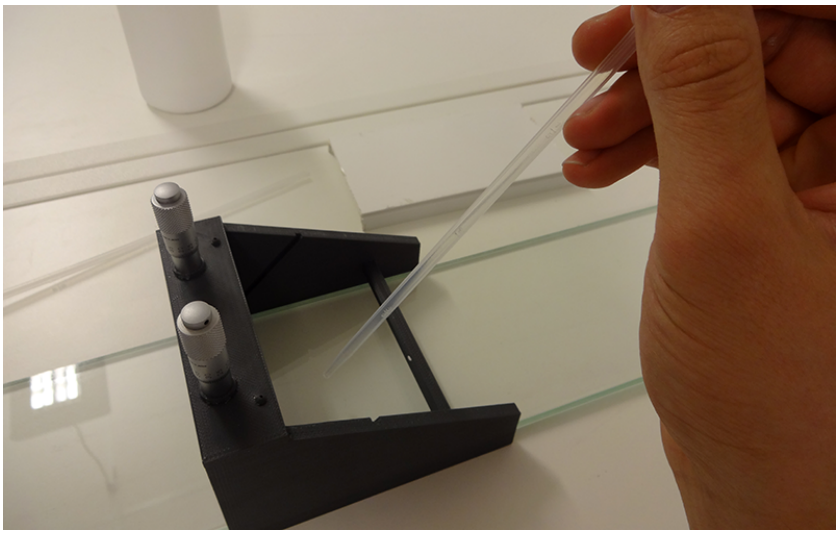

Figure A.7: Put the slurry in front of the applicator.

Collect slurry from the container with the pipet. When doing so, sink it close to the bottom of the container, to avoid sucking in air. When depositing the slurry on the plate, keep the pipet a bit above the plate. This will reduce the chance for producing bubbles in the slurry deposited. Do not do as in Figure A.8.

Figure A.8: Do not apply the slurry on to the plate in this manner. You are bound to get bubbles, which you do not want.

The better way of doing it is shown in Figure A.10. Nevertheless, if you do spot some bubbles in your film, you can suck them up with the pipet when it is emptied. On the other hand, I will not recommend it if you are co-casting, because there is a big chance of piercing both layers. Instead, use a needle or just a single copper thread from an electric wire to pop the bubbles.

Figure A.9: By keeping the pipet a bit above the slurry, you will reduce the chance of blowing air into it.

Assume a stable posture and put both hands on the applicator. Do not rest your arms on the applicator, it is only plastic and the weight from your hands can easily influence the structure and the position of the doctor blade. Push the applicator in a stable, slow and steady motion. Make sure that the glass plate is supported at the end, so that it will not move during the cast.

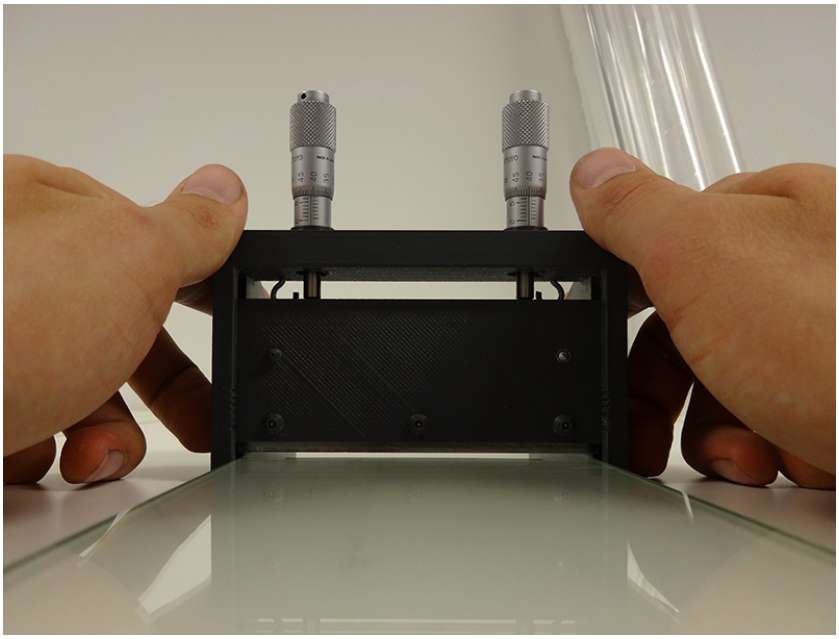

Figure A.10: Use both hand when dragging the applicator.

This should produce a uniform film without any remarkable imprints. By looking from an angle at the light reflections in the film, you will be able to spot any unevenness. It may be possible to "drag" the applicator several times across the slurry to make it more uniform, if the behavior of the slurry allows for it.

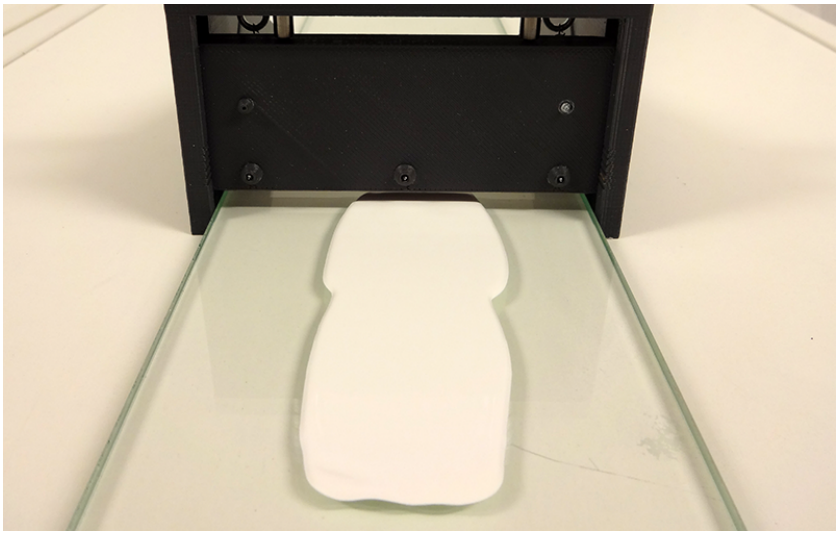

Figure A.11: After three depositions and three drags, the film was approved.

Depending on the slurry you are working with. If you have chosen a great share of alcohols to work as your slurry solvent, the chance is that the slurry can produce surface skin in a short amount of time. It will complicate the tape casting, requiring you to work very fast before it occurs. In this case, I recommend that you reduce the share of highly evaporative (solvents) alcohols and increase others, allowing you to work at a more comfortable pace. With a more user friendly slurry, you are able to polish the film, with several depositions and applicator drags. In a worse case, a second drag or an attempt to fix it in any way may ruin the film and render it useless.

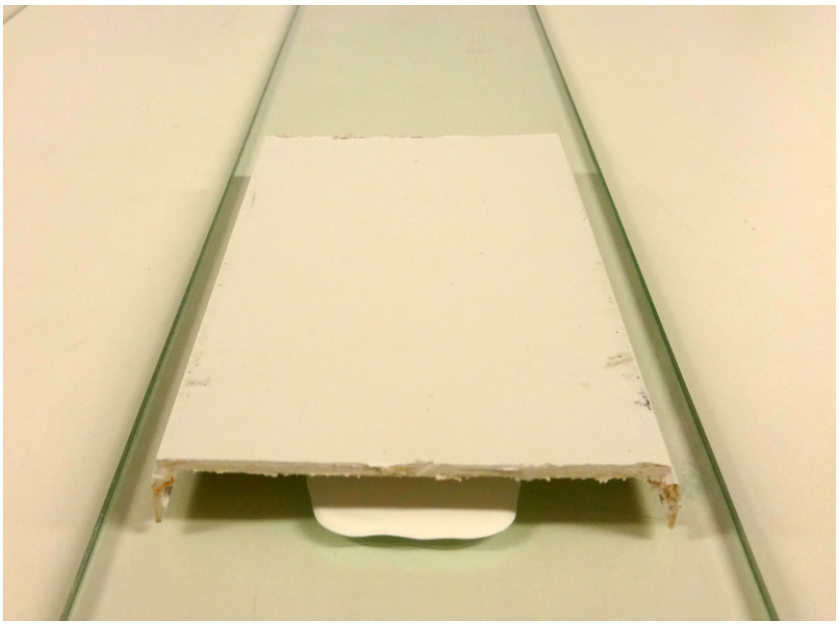

Figure A.12: Cover the tape when it is ready to dry.

When you are satisfied with the casted film, remember to cover it with something to reduce the amount of dust and particles to attach to it. Letting the film dry over night is usually sufficient for good results. As soon as you are finished, wash off the slurry from the doctor blade. Carefully rinse the blade under warm water, and dry of with paper.

Figure A.13: As sooner you clean the doctor blade, the easier it is.

You can test the dried tape by lifting some of it from the film carrier, use a finely edged spatula or something similar. If it tears before you are able to lift any of the carrier, it may not be ready or there is too little binder in the slurry formula.

When the film easily releases from the carrier it is ready to be shaped and further processed. It is important to have good routines on measuring and logging the samples you cut from the film, so that you can learn from shrinkage and changes which occur under sintering.

Figure A.14: Measure every sample you cut and shape, so that you are able to track any changes further on in the process, e.g. after sintering.

A.3 Preparation for Sintering

When sintering it is important to have support plates that are inert and does not react with the samples. But in most cases it could be smart to have some powder between the support plate and sample, underneath and on top. The samples often have a tendency to curl during sintering, which can be countered by having some weight on top to keep them flat. Resting the whole weight of a support plate on top of the samples are not strategic. With this much weight pressing down on the sample, can make the powder half sinter to the sample, or make the sample sinter to the support plate. If it sinters to the support plate, it takes a lot of work and time to sand of the sample. This is extremely time consuming and inefficient.

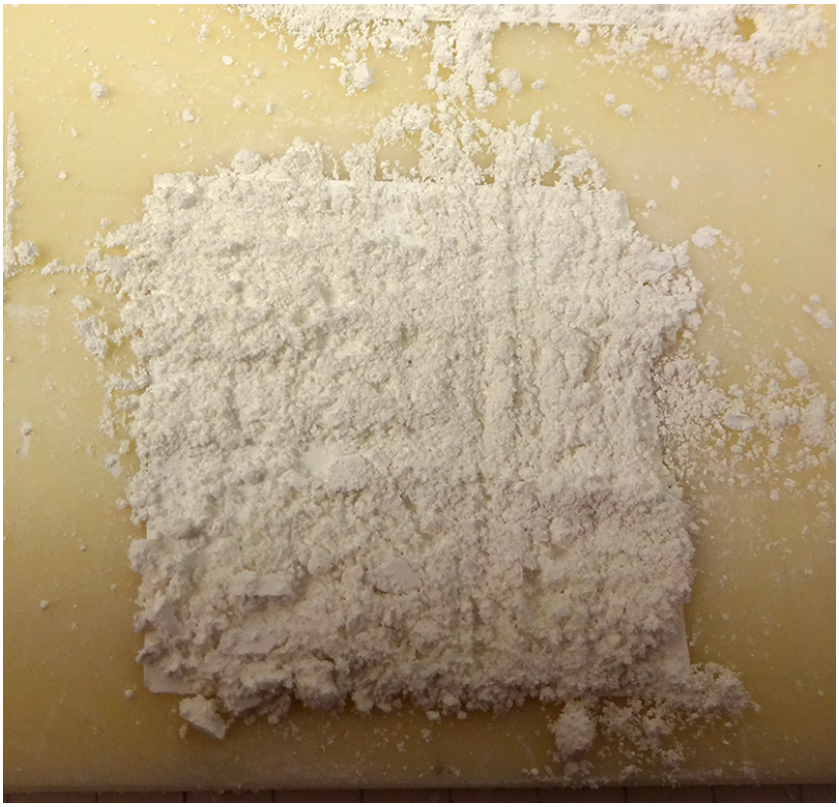

Figure A.15: Sample preparation for sintering.